Ferromagnetic correlations in bilayered $Sr_{3-x}Ca_xRu_2O_7$

Shin-ichi Ikeda

Department of Physics,
Faculty of Science,
Hiroshima University

February 1998

Abstract

We have synthesized a new bilayered ruthenate solid solution $Sr_{3-x}Ca_xRu_2O_7$ ($0 \leq x \leq 2.0$), which is homologous to copper-free layered perovskite superconductor Sr_2RuO_4 (T_c =1.5 K), with the aim of searching for new superconductors. We have also succeeded in growing single crystals of $Sr_3Ru_2O_7$ by a floating zone (FZ) method. A systematic measurement has been carried out for the x dependence of the lattice parameters, magnetic susceptibility $\chi(T)$, magnetization $M(H)$, and electrical resistivity $\rho(T)$. No indication of superconductivity has been observed down to 100 mK for x=0 (single crystals), 300 mK for x=1, and 2 K for other compositions. The measured values of lattice parameters and of magnetic quantities for the present single crystal samples are in good agreement with those for polycrystalline samples. Polycrystalline samples for $0.6 < x \leq 2.0$ show magnetic ordering below 50 K. It is intriguing that the magnetic correlations vary with increasing Ca content, from nearly ferromagnetic, to itinerant weakly ferromagnetic, and finally to localized antiferromagnetic. For x(Ca)=0, we have concluded that the ground state is the strongly-correlated Fermi liquid accompanied by enhanced ferromagnetic correlations. The lowest magnetic ordering temperature in this series is observed at 3.2 K in the sample with x(Ca) =1.0. This transition is described well as that due to a weakly ferromagnetic ordering by the self-consistent renormalization (SCR) theory of spin fluctuations. To the best of our knowledge, this is the first example to demonstrate an applicability of the SCR theory to a weak ferromagnet with a quasi-two dimensional crystal structure.

Contents

Chapter 1. Introduction

Since the discovery of high-T_c cuprate (copper oxide) superconductors (HTCS) [1] a decade ago, studies of HTCS have greatly improved our understandings of two-dimensional metallic states, strong electron-electron correlations, and antiferromagnetic spin fluctuations. Mainly two different perspectives have been discussed to explain the unusual behavior of HTCS. One approach starts from a localized electron system of the Mott insulator described, for example, in terms of the resonating valence bond (RVB) theory [2]. The other starts from an itinerant electron model including the self-consistent renormalization (SCR) theory [3] or Fermi liquid theory [4]. However, the exact mechanism of the high transition temperatures and anomalous metallic state above T_c have not been fully understood as yet.

The first superconductivity (SC) in non-cuprate layered oxides has been found [5] in Sr_2RuO_4, which motivated us to search for other SC compounds among ruthenates and other 4*d*-electron systems [6]. In spite of its low superconducting transition temperature of T_c=1.5 K, many intriguing aspects have been recognized in Sr_2RuO_4. There are, for example, the theoretical expectation of *p*-wave pairing symmetry [7-9] similar to the superfluid state of ^{3}He and the exotic SC state of heavy fermion compound UPt_3, experimental evidence for non-*s*-wave symmetry [10-13], two-dimensional Fermi liquid behavior [14], anomalous increase in T_c in Sr_2RuO_4-Ru hybrid system (3 K phase) [15], and so on. In addition, we have recently isolated a new ruthenate Mott insulator Ca_2RuO_4[16]. They are isostructural to Sr_2RuO_4 except for distortions present in Ca_2RuO_4. It is particularly interesting that Mott insulators are found in the vicinity of a superconductor not only for cuprates but also for ruthenates. In these ruthenates, strong electron-electron correlations appear to play a key role in determining their diverse properties as well as in cuprates.

A related ruthenate $Sr_3Ru_2O_7$, which has a tetragonal layered perovskite

structure (Fig.1), shows antiferromagnet-like cusp in the temperature dependence of magnetic susceptibility [6,17] around 15 K and nearly metallic behavior. We regard $Sr_3Ru_2O_7$ as a next candidate for SC ruthenate because of its two-dimensional RuO_2 bilayers, much weaker magnetic correlations than that of ferromagnetic $SrRuO_3$ (the Curie temperature T_c = 160 K) and the similarity in structure between HTCS $(La,Sr)_2CuO_4$ (T_c~40 K) and $(La,Sr)_2CaCu_2O_{6+\delta}$ (T_c~60 K) [18].

According to the band structure calculation of $Sr_3Ru_2O_7$ by Hase *et al.* [19], four Ru-4*d* electrons in the t_{2g} orbitals constitute low spin state with spin S=1 and mainly contribute to the density of states near the Fermi energy. Strong hybridization between Ru-4*d* in the t_{2g} orbitals and O-2*p* give rise to antibonding $pd\pi^*$ bands, a similar electronic state to that in Sr_2RuO_4 [20]. The resulting bands have six quasi-two-dimensional Fermi surfaces in $Sr_3Ru_2O_7$. Together with three quasi-two-dimensional Fermi surfaces in Sr_2RuO_4, these multi-bands near Fermi energy show a remarkable contrast with the single Fermi surface in HTCS. This orbital degeneracy in these ruthenates may play an important part in magnetism and transport properties.

The observation of zero-resistivity only in the single-crystalline Sr_2RuO_4 [5] obviously indicates that the study on good-quality single crystals is very important in searching for SC in ruthenates. Furthermore, investigations using single crystals are of crucial importance especially in extracting both anisotropic properties and intrinsic transport properties. In spite of some previous attempts [21] to grow large and high-quality single crystals of perovskite ruthenates by a floating-zone (FZ) method, successful growth had never been reported except for the superconducting Sr_2RuO_4.

In the present study, we have finally succeeded in growing single crystals of $Sr_3Ru_2O_7$ by the FZ method using high oxygen pressure. Physical properties of these single crystals are in good agreement with those of polycrystals. Just prior to our crystal growth, Cao *et al.* have investigated remarkable magnetic

and transport properties of Ruddelsden-Popper (R-P) type ruthenates $(Sr,Ca)_{n+1}Ru_nO_{3n+1}$ with n=1,2,3 and ∞ using single crystals grown by a chlorine flux method [22-27]. They have concluded that the ground state of $Sr_3Ru_2O_7$ [22] and $Ca_3Ru_2O_7$ [23] are an itinerant ferromagnet and a nonmetallic antiferromagnet, respectively. Lattice parameters and magnetic behavior of these flux-method crystals, however, are inconsistent with those of both polycrystals [28] and our single crystals grown by the FZ method. The discrepancies are especially serious in $Sr_3Ru_2O_7$, as we will describe below. The origin of the discrepancies has not been understood at present, but the difference in stoichiometry or inclusions of impurity elements may play a crucial role. Therefore, we believe that the data obtained from polycrystals gives important complementary information to those of the single crystals grown by the flux-method.

In order to modify the magnetic correlations and search for the SC ground state, we have performed substitution of smaller Ca cation into Sr sites in polycrystalline $Sr_{3-x}Ca_xRu_2O_y$ (SCRO) with x up to 2.0 [28].

In this paper, we will show that a sharp change in the magnetic properties occurs at x≈0.7 and x≈1.2, accompanied by the change in the lattice parameters in SCRO. We will also clarify a salient difference in the physical properties of single crystals $Sr_3Ru_2O_7$ associated with different crystal-growth methods. In addition, we suggest that the ground state of $Sr_3Ru_2O_7$ is a nearly ferromagnetic and strongly correlated Fermi liquid. We will conclude that the magnetism around x=1.0, where the lowest magnetic ordering temperature is observed, is well described by means of the self-consistent renormalization theory (SCR) of ferromagnetic spin fluctuations.

Chapter 2. Experimental

2.1 Sample preparation and characterization

For the synthesis of polycrystalline SCRO, we used a conventional solid-state reaction method. Stoichiometric mixtures of powders of $SrCO_3$ (99.99 %), $CaCO_3$ (99.99 %) and RuO_2 (99.9 %) were ground and calcined in air for 24 h at 1173 K. The calcined samples were reground and pressed into pellets. They were then reacted and sintered in a flow of a weakly reducing gas mixture (99 % Ar and 1 % O_2) at 1473 K for 24 h and cooled in the furnace. The procedure was repeated at 1573 K and 1623 K to obtain "as-prepared" samples. The reducing atmosphere is necessary to obtain SCRO phases. For example, firing the sample with x(Ca) = 1.5 in a flow of 0.1 MPa O_2 at 1623 K results in decomposition into (Sr,Ca)O and unidentified phases. Some as-prepared samples were then oxidized by annealing at 773 K under an oxygen atmosphere at relatively high pressure (1 and 5 MPa). For annealing at 773 K, ambient O_2 pressure was not adequate to prepare homogeneously oxidized samples because it resulted in the broadening of the peaks in the powder x-ray diffraction patterns, while 1 MPa O_2 annealing sustains the homogeneity of the samples.

The single crystals of $Sr_3Ru_2O_7$ were grown by the floating-zone (FZ) method. The starting materials were $SrCO_3$ with purity of 99.99% (Ba<5ppm) and RuO_2 with 99.9%. The mixture in the molar ratio of Sr:Ru=3:2.25 was fired and sintered in air at 1573 K with an intermediate grinding. The excess RuO_2 was added because of the high vapor pressure of Ru oxides at high temperature during the crystal growth. After being pressed into a rod with a diameter of 6 mm, it was sintered in air at 1623 K for 2 hours. The rod was then set in the FZ furnace (Nichiden Machinery : SC-K15HD-HP). The growth of crystals was performed in 1 MPa oxygen atmosphere at the feed speed of

40 mm/h. The rod and seed crystal were oppositely rotated each other at 30 rpm.

The crystal-growth atmosphere should be kept at high oxygen pressure because of the instability of RuO_2 at high temperatures as described below. The Sr_2RuO_4-Ru metal hybrid system, so-called 3 K phase [15], has been described by the eutectic solidification at the solidus line in the SrO-Ru phase diagram in 0.1 MPa air (~20 kPa oxygen partial pressure). This means that $Sr_3Ru_2O_7$ and $SrRuO_3$ do not exist in 0.1 MPa air at higher temperatures than the melting point (solidus line) in the SrO-Ru (not RuO_2) phase diagram.

As shown in the phase diagram (Fig. 2), RuO_2 is decomposed into Ru and oxygen at higher temperatures or at lower oxygen partial pressures [29-32]. In other words, high oxygen pressures stabilize RuO_2 with tetravalent oxidation state Ru^{4+} at high temperatures. Considering that formal valence number of Ru ion is also four in the R-P type ruthenates, it is necessary to stabilize RuO_2 at higher temperatures (~2200 K) than melting point during crystal growth by applying high oxygen pressures (~1.3 MPa) to obtain single crystals of $Sr_3Ru_2O_7$ or $SrRuO_3$. Therefore, we have tried to grow single crystalline $Sr_3Ru_2O_7$ at 1 MPa oxygen pressure, which is the maximum pressure for our FZ furnace.

2.2 Measurements

The crystal structures of the samples at room temperature were characterized by powder x-ray diffraction. The oxygen content y was determined by the thermogravimetric analysis (TGA). The temperature dependence of magnetic susceptibility $\chi(T)$ from 2 K to 350 K mostly under 1 T, the field dependence of magnetization $M(H)$ up to 5 T, and the AC magnetization with the frequency of 1 kHz and the amplitude of 0.1 mT were all measured by a superconducting quantum interference device (SQUID) magnetometer (Quantum Design, model MPMS-5S). We used sintered-bar samples with the weight of 10-50 mg. For magnetization measurements of single crystalline $Sr_3Ru_2O_7$, we performed sample rotation around the horizontal axis by the rotator equipped in MPMS-5S. We can make the crystal axes exactly parallel to a field direction within 0.2 degree by using this horizontal rotator. The electrical resistivity $\rho(T)$ was measured by a standard four terminal DC technique from 4.2 K to 300 K. The specific heat C_P of $Sr_3Ru_2O_7$ was measured by the adiabatic heat pulse method from 1.2 to 25 K using the sample pellet with a diameter of 12 mm and the weight of about 2.5 g. The AC susceptibility down to 0.1 K and 0.3 K was measured by a mutual-inductance method using a commercial dilution refrigerator (Oxford, Kelvinox-25) and a commercial ^{3}He refrigerator (Oxford, Heliox), respectively.

Chapter 3. Phase diagram of $Sr_{3-x}Ca_xRu_2O_7$

3.1 Lattice parameters and oxygen content

Powder x-ray diffraction spectra of as-prepared SCRO are shown in Fig. 3 for different x(Ca). The samples are essentially of single phase in the region $0 \leq x \leq 2.0$, although very weak impurity peaks of Sr_2RuO_4 are detected in the spectra of the samples with $0 \leq x \leq 0.6$. The spectra are well indexed in terms of the symmetry of tetragonal *I4/mmm* group up to x=2.0. It is clear that the solubility range of Ca in $Sr_3Ru_2O_7$ is considerably wide although the ionic radius of divalent Ca is substantially smaller than that of Sr. Lattice parameters for both as-prepared and oxidized samples determined from the x-ray diffraction spectra are plotted in Fig. 4. As we shall see below, three regions of distinct phases are clearly recognized : I($0 \leq x \leq 0.6$), II($0.6 < x \leq 1.2$) and III ($1.2 < x \leq 2.0$). Reflecting the smaller size of Ca ions, the unit cell volume exhibits nearly linear contraction with increasing x for $0 \leq x \leq 2.0$. With increasing x, monotonic decrease in the c parameter is observed except for samples in the region II around x =1.0. The crystal structure in the region II is characterized by abrupt shortening of the a parameter by about 0.5 % and stretching of the c parameter by about 1.0 %. In Fig. 4, we also included the lattice parameters of single crystals and polycrystals reported by several groups as described in Chapter 4.

For the investigations of crystal structures and electronic configuration, it is important to determine the oxygen content. We decomposed powders of the as-prepared sample into SrO, CaO and Ru in an alumina crucible by heating up to 1473K at 2 K/min under the atmosphere of flowing Ar with 10 % H_2 in a commercial TGA equipment. Before decomposing the samples, we dried both samples and alumina crucibles at 473 K in air for half an hour. The results give the oxygen content y in $Sr_{3-x}Ca_xRu_2O_y$ to be 6.95±0.06 for x=0, 6.99±0.06 for x=1.0 and 7.01±0.05 for x=2.0, indicating that y is essentially

7.0. This implies that the formal valency of Ru ion remains tetravalent with four 4*d* electrons. Therefore the observed structural changes by Ca substitution are not driven by the change in oxygen content. Lattice distortions of polycrystalline $Sr_3Ru_2O_7$ has been examined by Inoue *et al.* [33] using transmission electron microscopy. They reported the evidence for rotation of the RuO_6 octahedra by about 1 degree around the *c*-axis, with the direction of the rotation alternating from one layer to another within the bilayers. The existence of the rotation of the RuO_6 octahedra is in contrast with the absence of any lattice distortion in Sr_2RuO_4 down to low temperatures [34,35]. Neutron diffraction measurements on our samples by Morii *et al.* [36] suggest that Sr(Ca) atomic ordering does not occur in polycrystalline $Sr_2CaRu_2O_7$.

Oxidation effects on the lattice parameters are observed as shown in Fig. 4. For $x = 1.5$, annealing in 1 MPa O_2 results in the increase in the *c* parameter by 0.63 % and the decrease in the *a* parameter by 0.54 %. The increase in the oxygen content Δy inferred from the sample weight is 0.25 (y=7.25). The excess oxygen atoms are probably positioned at interstitial sites within the rock-salt $(Sr,Ca)_2O_2$ layers. The same tendency is observed for $x = 2.0$. On the other hand, for $x = 1.0$, the *c* parameter decreases by 0.45 %, the *a* parameter slightly increases by 0.18 % and Δy=0.10 (y=7.10) upon annealing in 5 MPa O_2 atmosphere. This behavior indicates that the oxidation effects in the region II and III are quite different. It is also remarkable that oxidation of samples in the region III noticeably reduce the unit cell volume, which is not seen in the region II.

3.2 Resistivity

The electrical resistivities $\rho(T)$ of the as-prepared polycrystalline samples are shown in Fig. 5. Metallic temperature dependence is observed for x = 0, and $d\rho/dT$ substantially increases below 20 K. This behavior is nearly consistent with ρ_{ab} and ρ_c of FZ single crystals of $Sr_3Ru_2O_7$ as explained in Chapter 4. Metallic temperature dependence is also observed for x = 1.0, 1.5 and 2.0, although it changes to nonmetallic behavior at lower temperatures. Nevertheless, the measured values of ρ at 300 K are ρ =8~30 mΩcm for $0 \le x \le 2.0$, at least three orders of magnitude lower in comparison with the results of the polycrystalline insulators Ca_2RuO_4 [16] and Sr_2IrO_4 [37,38]. Therefore the nonmetallic behavior may be ascribed to grain-boundary resistance, and the intrinsic behavior may be metallic to lower temperatures.

3.3 Magnetic susceptibility

For polycrystals, the temperature dependence of the magnetic susceptibility $\chi(T) \equiv M/H$ under a field of 1 T, for both field cooling (FC) and zero field cooling (ZFC) processes, is shown in Fig. 6. For $0 \le x \le 2.0$, $\chi(T)$ is fitted well with the Curie-Weiss behavior above 200 K and shows a cusp below 50 K. A temperature T_{max} defined at maximum $\chi(T)$ varies with x as indicated by arrows in Fig. 6 and shown in the top frame of Fig. 7. In the region I except for x = 0, T_{max} weakly increases with increasing x. The samples in the region I contain ferromagnetic impurity phase $(Sr,Ca)RuO_3$ ($T_c \le 160$ K) with estimated amount of about 1.6% from the magnetization measurements for x=0, although it is not detected in the x-ray spectra. In the region II, T_{max} shows small values of 3-5 K and is nearly independent of x. Across the boundary ($x \approx 1.2$) from the region II to region III, T_{max} shows an abrupt increase. It increases up to 43 K (x = 2.0) with further increasing x. The peak feature around T_{max} in the $\chi - T$

curve in the region III is suppressed by a field of 5 T (Fig. 8), indicating that it is ascribed to weak antiferromagnetic ordering with small ferromagnetic components such as those induced by canted moments. Magnetization measurements under a weak magnetic field (< 10^{-3} T) indicated no sign of superconductivity above 2 K in all the as-prepared and oxidized samples.

We fitted the data of $\chi(T)$ between 200 and 350 K with $\chi(T)=\chi_0+\chi_{CW}(T)$ (χ_0 : the temperature independent term, $\chi_{CW}(T)= C/(T-\Theta_W)$: the Curie-Weiss term). Here C is the Curie constant and Θ_W is the Weiss temperature. The effective Bohr magneton number p_{eff} is deduced from $C=N_A p_{eff}^2 \mu_B^2/3k_B$, where N_A is the Avogadro number, μ_B is the Bohr magneton and k_B is the Boltzmann constant, are shown in Fig. 7. We do not show p_{eff} and Θ_W in the region I for polycrystals because the data in the region I clearly contain the contribution from the ferromagnetic impurity (Sr,Ca)RuO_3. Assuming that Ru^{4+} is in the low spin state in the tetragonal crystalline electric field $t_{2g}^4 e_g^0$ (S=1) and that the orbital moment is quenched, we expect p_{eff} to be $g[S(S+1)]^{1/2}$ = 2.83, if the spins are localized. As shown in the bottom of Fig. 7, the observed p_{eff} remains almost constant (p_{eff}~2.7). The fair agreement of the p_{eff} values are somewhat fortuitous since we are dealing with itinerant-electron system here. Nevertheless the constancy of p_{eff} is consistent with the TGA results that the effective valence of Ru ion in SCRO changes little by Ca substitution. On the other hand, the inverse susceptibility χ^{-1} of samples with x = 1.0 and 2.0 as a function of T shown in Fig. 9 clearly indicates that the magnetic correlations of SCRO change with increasing Ca content. Because of the constancy of formal valence of Ru, this drastic change is quite possibly related to the structural modifications. Since the a parameter is almost constant but the c parameter shrinks rapidly with increasing x except in the region II, the change of magnetic correlations may have a relation to the change of c parameter.

Similar variation of the magnetic correlation is well known in (Sr,Ca)RuO_3 [39]. With substitution of Ca into $SrRuO_3$, magnetic correlation changes from

ferromagnetic to antiferromagnetic at $Sr_{0.4}Ca_{0.6}RuO_3$, despite the constancy of the formal Ru valency. In this three-dimensional system, only $SrRuO_3$ shows ferromagnetic ordering, while no magnetic ordering occurs in compounds with antiferromagnetic Weiss temperatures such as $CaRuO_3$ and $LaRuO_3$ [40]. Recent study of single crystalline $(Sr,Ca)RuO_3$ by Cao *et al.* [25] suggests that $Sr_{0.05}Ca_{0.95}RuO_3$, containing a very small amount of Sr, shows spin-glass-like ordering. It is noted that corresponding polycrystalline samples do not yield any magnetic ordering. The origin of such discrepancies between single crystals grown by the flux method and polycrystalline samples will be discussed in Chapter 4.

The temperature independent χ_0 is estimated at about $\pm 10^{-4}$ emu/Ru mol for $0 \leq x \leq 2.0$. Taking into account that core diamagnetic contribution is about -8×10^{-5} emu/f.u. mol, we estimate the Pauli paramagnetic contribution χ_{Pauli} to be rather small and at most 2×10^{-4} emu/Ru mol. This contrasts with a large Pauli contribution of nearly 1×10^{-3} emu/Ru mol for the superconductor Sr_2RuO_4.

It is noted that the difference in $\chi(T)$ between FC and ZFC is substantial in all the regions, especially strong in the region I. However, there is no such difference in $\chi(T)$ of the FZ crystals for $x=0$ as shown in Fig. 10. Therefore these indications of weak ferromagnetic ordering above T_{max} for polycrystals are probably not intrinsic. In the region III, a minimum in $\chi(T)$ below T_{max} is recognized for FC sequence as shown in Fig. 6. We therefore define another characteristic temperature T_{min} for this minimum, which shows gradual increase with increasing x up to 2.0.

3.4 AC magnetization

In order to detect T_{max} and T_{min} clearly, the real part of AC magnetization $M'(T)$ under almost zero field ($H_{DC} \leq 10^{-4}$ T and H_{AC}=0.1 mT) is displayed in Fig. 11. There exist two characteristic peaks in $M'(T)$ at temperatures T_1' and T_2', in addition to the ones ascribable to the ferromagnetic transition attributable to the impurity (Sr,Ca)RuO_3 and unidentified impurity phases. These temperatures are plotted against x (Fig. 12) by open circles and triangles. It is clear that T_1' is identified with T_{max}. According to the reports by Cao *et al.* [22,23], flux-method single crystalline $Sr_3Ru_2O_7$ ($Ca_3Ru_2O_7$) has two characteristic temperatures T^*=66 K and T_c=104 K (T_M=48 K and T_N=56 K). We also include these temperatures by open squares in Fig. 12. For Sr-rich compounds, some inconsistency of the characteristic temperatures as well as the lattice parameters is recognized between polycrystalline samples or FZ crystals (our work and that of Cava *et al.* [17]) and flux-method single crystals (Cao *et al.*). In particular, magnetic features at T_{max} and T_1' have not been recognized for the flux-method single crystals. On the other hand, the data of single crystalline $Ca_3Ru_2O_7$ appears consistent with the extrapolation of the data of polycrystalline SCRO. The T-x diagram suggests that T_{max} and T_{min} in the region III correspond to T_N and T_M, respectively, of flux-method single crystalline $Ca_3Ru_2O_7$. We will also discuss magnetic phases in the T-x diagram later. We have also measured the AC susceptibility of polycrystals for x=0 and 1.0 down to 0.3 K but proved negative evidence for superconductivity.

3.5 Magnetization curves

The nature of magnetism can be clarified from the field dependence of magnetization $M(H)$. Figure 13 shows $M(H)$ for the samples with different x at 2 K, below any magnetic ordering temperatures. It should be noted that the curvature of $M(H)$ for x = 1.0 is quite different from those for x = 0 and 2.0. With increasing applied field, $M(H)$ of x = 1.0 reveals saturation behavior. On the other hand, such saturation is not observed in $M(H)$ of x = 0 and 2.0, suggestive of metamagnetic transition at higher fields. $M(H)$ data of these three samples all show hysteresis. The magnitude of M(5 T) increases with increasing x(Ca). This implies that localized character of Ru-4*d* electrons in the ground state is enhanced in the Ca-rich phase, although its resistivity is metallic at high temperatures (T>200 K) and its magnetic moment is still only about one forth of what is expected for the localized Heisenberg spin system.

Now let us consider the relation between structural instability and Ru-4*d* electron states. Increasing the content of smaller Ca leads to contraction of the unit cell volume. By this contraction, stronger mixing between Ru-4*d* and O-2*p* electrons is naively expected. However, the results show the opposite tendency. The enhanced localized character with increasing x may be due to the reduction in the overlap of wave functions of Ru-4*d* and O-2*p* which is caused by the distortion of RuO_6 octahedra. This is analogous to the difference between metallic Sr_2RuO_4 and insulating Ca_2RuO_4 [16]. In addition, by oxidation of the samples in the region III, considered as the most distorted region, the *c* parameter increases, *a* parameter decreases, and the temperature of the antiferromagnet-like transition at T_{max} is depressed as shown in Fig. 14. This indicates that the distortions of RuO_6 octahedra are released by interstitial oxygen and are important for antiferromagnet-like transition in the region III.

At low temperatures, spin reorientation is often associated with structural phase transitions. To investigate whether the tetragonal crystal structure of

$SrCa_2Ru_2O_7$ changes below T_{min}, which corresponds to the metal-nonmetal transition in $Ca_3Ru_2O_7$, we have measured powder x-ray spectra at 4 K, which is well below T_{min}. The spectrum at 4 K is shown in Fig. 15 along with the result at 300 K. No symmetry change is observed from the spectra, although the *a* parameter elongates by 0.05% with lowering temperature down to 4 K, in contrast to the *c* parameter showing 0.55% shrink. This suggests that the effective increase of the *a* parameter, equivalent to Ru-Ru distance within the *ab*-plane, is associated with the metal-nonmetal transition. Recent structural study by Braden *et al.* [41] indicates that lattice distortions in orthorhombic Ca_2RuO_4 are described as the tiltings (rotations about in-plane axes) and rotations (rotations about the *c* axis) of rigid RuO_6 octahedra. In this SCRO system, exact structural refinements by neutron diffraction at low temperatures are needed to deepen the understanding of the ground state.

3.6 Phase diagram

In this section, we summarize the structural and magnetic phase diagram of $Sr_{3-x}Ca_xRu_2O_7$. Three regions I, II and III are well distinguished by the lattice parameters and magnetic ordering temperatures. For each region, there exist one or two characteristic temperatures as observed in the magnetization measurements. We give the interpretation of these temperatures below.

In the region I, T_{max} is not a definite magnetic ordering temperature as described in Chapter 4. In the region II, T_{max} is the Curie temperature characterized by itinerant weak ferromagnetism as described in Chapter 5. In the region III, T_{max} is antiferromagnetic transition temperature with canted ferromagnetism. According to the result of powder x-ray diffraction at 4 K for $SrCa_2Ru_2O_7$, T_{min} may correspond to spin reorientation temperature to greater canting without first order phase transition, which would have changed the symmetry of crystal structure. Ultimately, we can make the magnetic phase diagram of SCRO shown in Fig. 12. Structural study below characteristic temperatures of each phase will help confirming the interpretation given here.

Next, we discuss the distinction between three phases I, II and III. As analyzed in Chapter 5, the region II is well described by the itinerant weak ferromagnetism and is quite different from the others. This difference is also consistent with the singularity of x dependence of lattice parameters. The expectation of metamagnetic transition above a field of 5 T suggests that the magnetic ground state is rather localized in the region III than in the region II. As already described, the region III with enhanced lattice distortion should correspond to a more localized spin system than the region II. As a result, the magnetic ground states of $Sr_{3-x}Ca_xRu_2O_7$ system are characterized by the changeover from the itinerant weak ferromagnetism in the region II to the localized antiferromagnetic spin system in the region III with increasing x. For the region I, we will discuss the ground state based on the results of single crystalline $Sr_3Ru_2O_7$ in the following Chapter.

Chapter 4. $Sr_3Ru_2O_7$: nearly ferromagnetic metal

In this Chapter, we will describe the experimental results of $Sr_3Ru_2O_7$ using FZ single crystals and will present the evidence for a nearly ferromagnetic metal with the strongly correlated Fermi liquid ground state. We will also discuss the difference of $Sr_3Ru_2O_7$ synthesized by different methods reported by several groups.

The cleaved single-crystals of $Sr_3Ru_2O_7$ were obtained by crushing a bar-shape single crystal (5 mm$\phi\times$25 mm). The 327 structure was confirmed using crushed crystals by the powder x-ray diffraction spectra, which indicated no impurity peaks as shown in Fig. 16(a). Details of the crystal structure with atomic coordinates have been described elsewhere [19]. Lattice parameters at room temperature were deduced as a= 3.8872(4) Å and c=20.732(3) Å by assuming tetragonal *I*4/*mmm* symmetry. These values are in good agreement with those of polycrystals within an experimental error but show significant difference from the reported values for single crystals grown by a flux method [22] as described below. Figure 16(b) shows the (00ℓ) reflection spectrum from several pieces of cleaved plate-like crystals. All (00ℓ) peaks allowed for the tetragonal symmetry are clearly observed and the corresponding c parameter (c=20.741 Å) is consistent with that obtained from the powder diffraction spectra. This is strong evidence that the cleaved surface is a two-dimensional *ab*-plane.

The temperature dependence of magnetic susceptibility $\chi_{ab}(T)$ and $\chi_c(T)$ in the field of 0.3 T is shown in Fig. 17. Little magnetic anisotropy is observed in contrast to large anisotropy (~10^2) of crystals grown by a flux method [22]. This nearly isotropic susceptibility of $Sr_3Ru_2O_7$ is similar to that of the enhanced Pauli-paramagnetic behavior in Sr_2RuO_4 [14]. Around T_{max} =17 K, $\chi_{ab}(T)$ and $\chi_c(T)$ show a cusp without ferromagnetically ordered components. This behavior is almost the same as that of polycrystals [6,17]. Below 5 K, both $\chi_{ab}(T)$ and

$\chi_c(T)$ are temperature independent and completely isotropic. Furthermore the susceptibilities below 5 K retain a quite large value (~1.5×10^{-2} emu/mol Ru).

Both $\chi_{ab}(T)$ and $\chi_c(T)$ exhibit the Curie-Weiss behavior above 200 K. We have fitted the observed $\chi_{ab}(T)$ and $\chi_c(T)$ with $\chi(T)=\chi_0+\chi_{CW}(T)$, where χ_0 is the temperature independent term and $\chi_{CW}(T) = C/(T-\Theta_W)$ is the Curie-Weiss term in the temperature range between 200 K and 350 K. The effective Bohr magneton numbers p_{eff} deduced from C are listed in Table 1 along with χ_0 and Θ_W. In Fig. 18, we show the field dependence of magnetization $M(H)$ for fields along the *ab*-plane and the *c*-axis at several temperatures. The magnetic moment at 5 T is at most 0.25 μ_B and no spin-flip reorientation is recognized up to 5 T. This means that simple localized spin system with a small exchange energy is not a plausible model for $Sr_3Ru_2O_7$. Furthermore, the magnetization curves show no hysteresis between increasing and decreasing field. Therefore, explicit ferromagnetically ordered moments never exist in $Sr_3Ru_2O_7$.

It is interesting to compare the enhanced Pauli-paramagnetic Sr_2RuO_4 and Curie-Weiss-like $Sr_3Ru_2O_7$. Recent theoretical and experimental results of Pauli-paramagnetic Sr_2RuO_4 suggest the possibility of spin-triplet pairing by ferromagnetic spin fluctuations in the superconducting state. The crystal structure of $Sr_3Ru_2O_7$ is more three-dimensional than that of Sr_2RuO_4. Considering that the formal valence of Ru ion is the same (Ru^{4+}), the major difference in the electronic properties between them probably originates from the dimensionality. $Sr_3Ru_2O_7$ exhibits a cusp at 17 K in $\chi(T)$, naively suggestive of antiferromagnetic correlations. On the other hand, further increase of three-dimensionality on $Sr_3Ru_2O_7$ leads to ferromagnetic metal $SrRuO_3$ (T_c=160 K) [42]. Other evidence for ferromagnetic correlations in $Sr_3Ru_2O_7$ is discussed later. Thus, the q-dependence of $\chi(q,\omega)$ must be such that both ferromagnetic (q=0) and antiferromagnetic ($q\neq0$) correlations are important.

Such a complicated magnetism has been studied in UPt_3. Inelastic neutron diffraction measurements [43] suggested a weak antiferromagnetic ordering

below T_N=5 K accompanied by a very small moment (~0.02 μ_B). However, at present, it has not been confirmed whether this anomaly at 5 K in UPt_3 corresponds to a static ordering or not [44]. At the same time, low temperature specific heat is described by a paramagnon mode i.e. ferromagnetic spin fluctuations [45]. The similarity between $Sr_3Ru_2O_7$ and UPt_3 may help clarifying the magnetism of each other. Although we had hoped that the FZ crystals of $Sr_3Ru_2O_7$ to exhibit SC below 1 K as UPt_3, AC susceptibility down to 100 mK resulted in negative evidence.

Temperature dependence of the electrical resistivity $\rho(T)$ is shown in Fig. 19 in the range between 4 and 300 K. Both $\rho_{ab}(T)$ and $\rho_c(T)$ are metallic ($d\rho/dT$ >0). The ratio of ρ_c/ρ_{ab} is about 160 at 4 K and 20 at 300 K. This anisotropic resistivity is consistent with the quasi-two-dimensional Fermi surface sheets obtained from the band structure calculations for $Sr_3Ru_2O_7$ [19]. In contrast to the T^2-dependence of both $\rho_{ab}(T)$ and $\rho_c(T)$ for Sr_2RuO_4, characteristic of a Fermi liquid, $Sr_3Ru_2O_7$ yields a complicated temperature dependence of resistivity. With lowering temperature below 100 K, a remarkable decrease of ρ_c is observed. Below 17 K where $\chi(T)$ shows a maximum, $\rho_c(T)$ appears to be proportional to T. On the other hand, $\rho_{ab}(T)$ shows a slight increase of $d\rho/dT$ and a quadratic temperature dependence below 7 K. We fitted $\rho_{ab}(T)$ by the formula $\rho_{ab}=\rho_0+A_{ab}T^2$ below 7 K and obtained ρ_0=5.9 $\mu\Omega$ cm and A_{ab}=0.14$\mu\Omega$ cm/K^2. Since the susceptibility is quite isotropic and temperature independent below 5 K as expressed above, the ground state of $Sr_3Ru_2O_7$ is a Fermi liquid. The resistivity measurements below 4 K will be required in order to define whether $\rho_c(T)$ shows T^2-dependence or not.

In order to clarify the magnetic anomaly at 17 K in $\chi(T)$ of $Sr_3Ru_2O_7$, the nuclear magnetic relaxation rate $1/T_1$ has been measured by Mukuda *et al.* using our polycrystalline samples (Fig. 20). At around 17 K, we can hardly observe any divergence in $1/T_1$. The experimental data suggests that the cusp at 17 K in $\chi(T)$ does not indicate a definite magnetic ordering. Nevertheless,

the substantial decrease in the Ru-nuclear relaxation rate below 17 K indicates that the amplitude of spin fluctuations is reduced by something or other. From the analysis of temperature dependence of Knight shift by Mukuda *et al*., it is concluded that short range antiferromagnetic ordering develops below 60 K.

Specific heat divided by temperature C_P/T is shown for polycrystalline $Sr_3Ru_2O_7$ in Fig. 21. It is noted that no clear peak is observed around T_{max}=17 K. Instead, the T^2 dependence of C_P/T does not follow the simple relation of $C_P/T = \gamma + \beta T^2$ below 17 K. As observed in Fig. 21, the deviation, i.e. additional entropy, may be due to the substantial development of short range antiferromagnetic ordering observed in the Knight shift. Below 4 K, the same region that Fermi liquid state is suggested, C_P/T shows a strong decrease. In the range of temperature between 400 $K^2 \leq T^2 \leq 800$ K^2, fitting the data using the formula above gives the Sommerfeld coefficient of γ = 63 mJ/Ru mol K^2 and β = 0.273 mJ/Ru mol K^4. The Debye temperature is evaluated as Θ_D = 350 K from $\beta = 12\pi^4 N k_B / 5\Theta_D^3$ where N=6 is half of the number of atoms in formula unit. The largest specific heat γ value of $Sr_3Ru_2O_7$ among the R-P type ruthenates (30 mJ/Ru mol K^2 for $SrRuO_3$ [46] and 38 mJ/Ru mol K^2 for Sr_2RuO_4 [14,47]) provides clear evidence that $Sr_3Ru_2O_7$ is a strongly correlated 4*d*-electron metallic oxide. A local-density electronic-band-structure calculation has been performed for $Sr_3Ru_2O_7$ by Hase and Nishihara [19]. They deduced the density of states at the Fermi energy $D(E_F)$=10.3 states/eV cell, corresponding to the electronic specific heat coefficient γ_{band}=12.1 mJ/Ru mol K^2. Thus the mass enhancement factor $\gamma_{exp}/\gamma_{band}$=5.2 surpasses that of Sr_2RuO_4 at $\gamma_{exp}/\gamma_{band}$=3.6 [14,20].

For estimating the magnetic contributions C_m from Ru-4*d* electrons to specific heat C_P, we subtracted the lattice part βT^3 from the raw data as $C_m = C_P - \beta T^3$. Magnetic entropy S_m is calculated by $S_m(T) = \int_0^T \frac{C_m}{T} dT$. Then, we obtain $S_m(T=17\text{ K}) = R\ln(2S_{eff}+1) = 1.4$ J/K Ru mol with R=8.31 J/K mol. The effective spin S_{eff} is about 0.09. This entropy is about 7 times smaller than S_m=9.13 J/K

mol for S_{eff}=1 corresponding to well localized $Ru^{4+}(4d^4)$ spins in the low spin state. Therefore magnetic anomaly at 17 K in $Sr_3Ru_2O_7$ is associated with a very small magnetic moment (~0.18 μ_B), similar to the weak antiferromagnetic correlations characterized by a small U-5*f* moment in UPt_3 [43].

It is important to note that even at temperatures much lower than 17 K, the magnetic susceptibility remains quite large. It appears that the ground state maintains a highly enhanced magnetic susceptibility of 1.5×10^{-2} emu/mol Ru. Considering that the observed magnetic susceptibility is due to the quasi-particle of Fermi liquid state, we can estimate the Wilson ratio $R_W=\pi^2k_B^2\chi_0/3\mu_B^2\gamma = 7.291\times10^8\chi_0/\gamma$ where χ_0 (in emu/Ru mol) is a magnetic susceptibility and γ (in erg/K^2 Ru mol) is a Sommerfeld coefficient of specific heat in the ground state, respectively. If we regard the observed χ at 2 K as that at 0 K, we obtain R_W =17.4. This value of R_W much larger than unity implies that ferromagnetic correlations are strongly enhanced in this compound. Such a ground state is known as a nearly ferromagnetic metal. In addition, we can also estimate Kadowaki-Woods ratio A/γ^2, where A is the resistivity coefficient of T^2 in Fermi liquid state. For $Sr_3Ru_2O_7$, assuming that electronic specific heat is mainly due to the *ab*-plane component, we obtain $A/\gamma^2\approx A_{ab}/\gamma^2=3.5\times10^{-5}\mu\Omega$ cm/(mJ/K^2mol Ru)^2 similar to that observed in heavy fermion compounds as shown in Fig. 22. These results indicate that the ground state of $Sr_3Ru_2O_7$ is a strongly correlated Fermi liquid with the enhanced ferromagnetic correlations. At high temperature around 17 K, magnetic excitations are dominated by the short range antiferromagnetic correlations. Therefore we conclude that $Sr_3Ru_2O_7$ is a nearly ferromagnetic metal based on the strongly correlated Fermi liquid as the ground state and exhibiting antiferromagnetic excitations at high temperatures.

Now we discuss the distinction of lattice parameters, susceptibility and resistivity among different synthesis methods of polycrystalline and single crystalline $Sr_3Ru_2O_7$. Lattice parameters reported by Müller-Buschbaum *et al.*

[48], Cao *et al.* [22,24] and Cava *et al.* [17] as well as ours are shown in Fig. 23. Systematic difference in the *c* parameter between the flux-method and others is recognized. The flux-grown single crystals show a clear ferromagnetic transition at T_c=104 K and its ordered moment below T_c is about 1.3 μ_B/Ru even under a weak magnetic field $\mu_0 H$=0.3 T along the *c*-axis [22]. On the other hand, FZ crystals do not exhibit any ferromagnetic ordering and its moment under $\mu_0 H$=0.3 T is about 0.01 μ_B/Ru along both *ab*-plane and *c*-axis at 10 K. Temperature dependence of resistivity of flux-grown single crystals is nearly the same as that of FZ crystals. However, the absolute value for flux-grown single crystals is about 8 times larger than that of FZ crystals. The 5% doping of non-magnetic Th into UPt_3 is known to cause an obvious change in lattice parameters, 0.2% decrease in the unit cell volume [49], and clear spin density wave ordering at 6.5 K [50], which is never observed in pure UPt_3. Considering that the present-FZ method can prevent crystals from containing the impurity above 0.1% level, possibility of inclusions in flux-method crystals of $Sr_3Ru_2O_7$ should be worth investigation in future study.

Chapter 5. $Sr_2CaRu_2O_7$: weakly ferromagnetic metal

The SCRO system shows both the Curie-Weiss behavior of magnetic susceptibility and non-insulating electrical resistivity. Similar properties were observed in the mixed metallic phase $(Sr,Ca)RuO_3$ and were discussed in terms of the self-consistent renormalization theory (SCR theory [3,51]) as an itinerant ferromagnet [52]. The SCR theory based on the antiferromagnetic spin fluctuations has been applied also to HTCS in order to understand both superconducting symmetry and normal state properties [3]. Spin fluctuations for a weak ferromagnet should be an appropriate picture for analyzing the magnetism in SCRO, especially in the region II where very low T_{max} (3-5 K) is observed.

The SCR theory is based on the relation between magnetic free energy F_m per one magnetic ion and the dimensionless magnetization p as follows:

$$F_m = \frac{r}{2}p^2 + \frac{\bar{F}_1}{4}\left(\frac{p}{2}\right)^4, \qquad (1)$$

where $p = M(H,T)/\mu_B N_A$, r and $\bar{F}_1$ represent the second and the fourth order expansion coefficient, respectively. Especially, $\bar{F}_1$ has an substantial meaning as the mode-mode coupling constant among spin fluctuations with different wave vector $\boldsymbol{q}$. Considering that thermodynamically stable state can be deduced from the first derivative of Eq. (1), we obtain the following equation.

$$\frac{16\mu_B}{\bar{F}_1}\frac{H}{p} = p^2 - p_S{}^2, \qquad (2)$$

where spontaneous magnetization $p_S = p(T=0\ \text{K}, H=0\ \text{Oe})$.

The Arrott plot of magnetization curves (p^2 vs H/p) for $x = 1.0$ at different temperatures is shown in Fig. 24. The appearance of the positive intercept on the vertical axis indicates that the intrinsic Curie temperature T_c is below 5 K.

Therefore we identify T_{max}=3.2 K as the intrinsic Curie temperature T_c. Only the data in the region II satisfy the relation that p^2 is proportional to H/p. The spontaneous magnetization p_S should be somewhat larger than observed p(T=2 K, H=0 Oe)=0.08. However it is suggested that p_s is much smaller than p_{eff} = 2.82 evaluated from χ (T). These characterize SCRO in the region II as a weak ferromagnet.

For itinerant electron systems, magnetic anisotropy is not substantial in comparison with localized electron systems, since magnetic correlation length of the itinerant spins is considerably longer than that of the localized spins. For region II, the low Curie temperature of ~10^0 K indicates that magnetic anisotropy energy is at most 10^{-2}-10^{-1} K. Thus the observed magnetization $p(H)$ up to 5 T (Fig. 24) for the polycrystalline samples should reflect the intrinsic process, rather than the average of two strongly anisotropic contributions. Nevertheless, a recent theory by Hatatani and Moriya [53] discusses a subtle difference in the behavior of the isotropic two-dimensional system of spin fluctuations from that of the isotropic three-dimensional system.

In weakly ferromagnetic metals, the SCR theory gives another relation:

$$\frac{p_S^2}{4} = \frac{15T_0}{T_A} c \left(\frac{T_c}{T_0}\right)^{\frac{4}{3}}, \qquad (3)$$

where c=0.33536 is a constant, T_c is the Curie temperature, and T_0 and T_A characterize the energy width of the dynamical spin-fluctuation spectrum and the width of the distribution of the static susceptibility in the $\boldsymbol{q}$-space, respectively. T_0 and T_A correspond to the exchange energy J in the localized spin system. The ratio of T_A/T_c much larger than unity means that spin fluctuations only near $\boldsymbol{q}$=0 contribute to the magnetic ordering.

We consider the relation derived by Takahashi [54]:

$$\bar{F}_1 = \frac{4k_B T_A^{\,2}}{15T_0}. \qquad (4)$$

$\bar{F}_1$ can be derived from the gradient of the Arrott plot using Eq. (2).

It is not very precise to estimate the spontaneous magnetization p_S (T=0 K, H=0 Oe) from the data of $p(H)$ at 2 K because this temperature cannot be regarded as much below T_c=3.2 K. Therefore, we regard p_S as a fitting parameter and fit the inverse magnetic susceptibility in the limit of zero field, $\chi^{-1}(T, H=0\ \mathrm{Oe})$, using the following relations in order to determine the SCR parameters as in Ref. [55]. Assuming the weakly ferromagnetic limit, i.e. T_c/T_0 «1, we can simplify the relations as follows:

$$y = \frac{\bar{F}_1 p_s^{\,2}}{8T_A \eta^2}\left\{-1 + \frac{1+\nu y}{c}\int_0^{\frac{1}{\eta}} dz \cdot z^3\left[\ln u - \frac{1}{2u} - \Psi(u)\right]\right\}, \qquad (5)$$

with

$$y = \frac{N_A}{2T_A \chi \eta^2}, \qquad (6)$$

$$\eta = \left(\frac{T_c}{T_0}\right)^{\frac{1}{3}}, \qquad (7)$$

$$\nu = \frac{\eta^2 T_A}{U}, \qquad (8)$$

$$u = \frac{z(y+z^2)}{t}, \qquad (9)$$

where $\Psi(u)$ is the digamma function, U is the intra-atomic exchange energy and $t=T/T_c$. Using these relations and assuming $U=10^4$ K, we can predict $\chi(T,H=0\ \mathrm{Oe})$ above T_c for several values of p_S as shown in Fig. 25. For experimental $\chi(T,H=0\ \mathrm{Oe})$ we employ positive intercepts in the Arrott plot (Fig. 24) where the line of extrapolation of high field data crosses the horizontal

axis. Adequate reproduction of $\chi(T,H=0$ Oe) is obtained when p_S is 0.2. Furthermore, T_0 and T_A are evaluated self-consistently from Eqs. (3), (4) and (5). All the SCR parameters thus evaluated are, T_c = 3.2 K, p_S = 0.2, $\bar{F}_1$ = 433 K, T_0 = 133 K and T_A = 465 K.

The ratios T_c/T_0=0.0241 and p_{eff}/p_s=14.1 are important for the classification of the itinerant/localized ferromagnets. Figure 26 is based on the generalized Rhodes-Wohlfarth plot (p_{eff}/p_s vs T_c/T_0) for weak ferromagnets by Takahashi [54]. In the original Rhodes-Wohlfarth plot , p_{eff}/p_s is plotted against T_c. In this plot, large p_{eff}/p_s and small T_c/T_0 represents the strong itinerant character of electrons. The localized Heisenberg system is characterized by $p_{eff}/p_s = T_c/T_0$=1. $Sr_2CaRu_2O_7$ (x=1.0) is regarded as a weakly ferromagnetic metal with intermediate character as shown.

For polycrystalline $Sr_{0.4}Ca_{0.6}RuO_3$, Kiyama *et al.* [52] obtained T_c =25 K and $T_A \approx$ 5000 K from $M(H)$, thus $T_A/T_c \approx$ 200. A similar value of T_A/T_c=145 for $Sr_2CaRu_2O_7$ indicates that the similar weak ferromagnetism occurs in both compounds despite the difference in dimensionality of Ru-O network. Our study is probably the first example of applying the SCR theory to ferromagnet with a quasi-two-dimensional layered crystal structure [53]. Theoretical modification of Takahashi's relation [Eq. (4)] for a quasi-two-dimensional system should be required in order to advance the investigation of the two-dimensional weak ferromagnet. Nevertheless it is expected that the analysis presented here remains qualitatively valid also for systems with two-dimensional ferromagnetic spin fluctuations [56].

The strong ferromagnetic spin fluctuations in $Sr_2CaRu_2O_7$ implies that similar ferromagnetic correlations are present also in $Sr_3Ru_2O_7$. All the results point toward the presence of ferromagnetic correlations in Sr-Ru-O R-P phases. Hence further study of Sr-Ru-O R-P phases will provide the dimensionality dependence of ferromagnetic correlations and will help searching for other two-dimensional ferromagnets.

Chapter 6. Conclusion

In conclusion, we have characterized the magnetic and structural properties of the new bilayered ruthenate series $Sr_{3-x}Ca_xRu_2O_y$ ($0 \leq x \leq 2.0$). The oxygen content y has been determined as essentially 7.0 for all x before annealing in the oxidizing atmosphere. In addition, we have firstly succeeded in growing large and high quality single crystals of $Sr_3Ru_2O_7$ by the floating-zone method. The results of magnetization, resistivity and specific heat measurements suggest that $Sr_3Ru_2O_7$ is a strongly correlated Fermi liquid with nearly ferromagnetic ground state. The magnetic properties in the region around x=1.0 are associated with the appearance of the itinerant weak ferromagnetism. On the basis of the SCR parameters $Sr_2CaRu_2O_7$ is classified as the first weak ferromagnet with quasi-two-dimensional crystal structure. With increasing Ca, the ground state of SCRO changes dramatically from nearly ferromagnetic and strongly correlated Fermi liquid, to weakly ferromagnetic metal, and finally to localized antiferromagnetic spin system.

Acknowledgments

The author wishes to express his sincere thanks to Professor Toshizo Fujita for stimulating discussion and critical advice. He appreciates Associate Professor Yoshiteru Maeno for being a great help during his research days at Kyoto University. He thanks Hiroshi Muranishi, Shuji Nishizaki, Satoru Nakatsuji, Yasumitsu Mori, Takashi Ando and Zhiqiang Mao for valuable discussions and greatly acknowledge Professor Takehiko Ishiguro and the members of Ishiguro's laboratory for their supports. He is grateful to Associate Professor Kazuyoshi Yoshimura, Mr. Takashi Kiyama, Professor Toru Moriya, and Professor Yoshinori Takahashi for their useful advice in analyzing the data using the SCR theory. He is grateful also to Professor Yasumasa Koyama, Dr. Gang Cao, Dr. Markus Braden, Dr. Yukio Morii, Dr. Yasuhide Inoue, Mr. Masayuki Hara, Professor Kazumasa Miyake and Professor Kosaku Yamada for their useful advice. He thanks Dr. Izumi Hase for discussing his band structure calculation results prior to publication. He acknowledges Dr. Andy Mackenzie for his collaboration with the author. He thanks Dr. Kenji Ishida and Mr. Hidekazu Mukuda for discussing their NMR results prior to publication. He thanks Mr. Kou-ichi Izawa, Miss Kimie Senami, Dr. Fumihiko Nakamura, and Associate Professor Takashi Suzuki for their help on everything in Hiroshima University. Some of the measurements were performed at the Cryogenic Center of Hiroshima University. He has also been a research student also for two years in Department of Physics, Graduate School of Science, Kyoto University. He really appreciates a lot of help during his school days by his family.

References

[1] J. G. Bednorz and K. A. Müller, Z. Phys. B **64**, 189 (1986).

[2] P. W. Anderson, Science, **235**, 1196 (1987).

[3] T. Moriya, Y. Takahashi, and K. Ueda, J. Phys. Soc. Jpn. **59**, 2905 (1990).

[4] S. Koikegami and K. Yamada, preprint.

[5] Y. Maeno, H. Hashimoto, K. Yoshida, S. Nishizaki, T. Fujita, J. G. Bednorz, and F. Lichtenberg, Nature **372**, 532 (1994).

[6] S. Ikeda, Y. Maeno, M. Nohara, and T. Fujita, Physica C **263**, 558 (1996).

[7] T. M. Rice and M. Sigrist, J. Phys. Cond. Matter, **7**, L643 (1995).

[8] M. Sigrist and M. E. Zhitomirsky, J. Phys. Soc. Jpn. **65**, 3452 (1996).

[9] K. Machida, M. Ozaki, and T. Ohmi, J. Phys. Soc. Jpn. **65**, 3720 (1996).

[10] S. Nishizaki, Y. Maeno, S. Farner, S. Ikeda, and T. Fujita, J. Phys. Soc. Jpn. **67**, 560 (1998).

[11] A. P. Mackenzie, R. K. W. Haselwimmer, A. W. Tyler, G. G. Lonzarich, Y. Mori, S. Nishizaki, and Y. Maeno, Phys. Rev. Lett. **80**, 161 (1998).

[12] K. Ishida, Y. Kitaoka, K. Asayama, S. Ikeda, S. Nishizaki, Y. Maeno, K. Yoshida, and T. Fujita, Phys. Rev. B**56**, R505 (1997).

[13] R. Jin, Yu. Zadorozhny, Y. Liu, Y. Mori, Y. Maeno, D. G. Schlom, F. Lichtenberg, and J. G. Bednorz, submitted to Nature.

[14] Y. Maeno, K. Yoshida, H. Hashimoto, S. Nishizaki, S. Ikeda, M. Nohara, T. Fujita, A. P. Mackenzie, N. E. Hussey, J. G. Bednorz and F. Lichtenberg, J. Phys. Soc. Jpn. **66**, 1405 (1997).

[15] Y. Maeno, E. Ohmichi, T. Ando, Y. Mori, S. Ikeda, S. Nishizaki, and S. Nakatsuji, preprint.

[16] S. Nakatsuji, S. Ikeda, and Y. Maeno, J. Phys. Soc. Jpn. **66**, 1868 (1997).

[17] R. J. Cava, H. W. Zandbergen, J. J. Krajewski, W .F. Peck, Jr., B. Batlogg, S. Carter, R. M. Fleming, O. Zhou, and L. W. Rupp, Jr., J. Solid State Chem. **116**, 141 (1995).

[18] R. J. Cava, B. Batlogg, R. B. van Dover, J. J. Krajewski, J. V. Waszczak, R. M. Fleming, W. F. Peck Jr., L. W. Rupp Jr., P. Marsh, A. C. W. P. James and L. F. Schneemeyer, Nature **345**, 602 (1990).

[19] I. Hase and Y. Nishihara, J. Phys. Soc. Jpn. **66**, 3517 (1997).

[20] T. Oguchi, Phys. Rev. B **51**, 1385 (1995).

[21] Y. Maeno, S. Nishizaki, K. Yoshida, S. Ikeda, and T. Fujita, J. Low Temp. Phys. **66**, 1405 (1997).

[22] G. Cao, S. McCall, and J. E. Crow, Phys. Rev. B **55**, R672 (1997).

[23] G. Cao, S. McCall, J. E. Crow, and R. P. Guertin, Phys. Rev. Lett. **78**, 1751 (1997).

[24] G. Cao, S. C. McCall, J. E. Crow, and R. P. Guertin, Phys. Rev. B **56**, 5387 (1997).

[25] G. Cao, S. McCall, M. Shepard, J. E. Crow, and R. P. Guertin, Phys. Rev. B **56**, 321 (1997).

[26] G. Cao, S. McCall, M. Shepard, J. E. Crow, and R. P. Guertin, Phys. Rev. B **56**, R2916 (1997).

[27] G. Cao, S. K. McCall, J. E. Crow, and R. P. Guertin, Phys. Rev. B **56**, R5740 (1997).

[28] S. Ikeda, Y. Maeno, H. Muranishi, and T. Fujita, J. Low Temp. Phys. **105**, 1599 (1996).

[29] D. Chatterji and R. W. Vest, J. Am. Ceram. Soc., **54** (2) 73 (1971).

[30] S. Pizzini and L. Rossi, Z. Naturforsch., **26A** (1) 177 (1971).

[31] W. E. Bell and M. Tagami, J. Phys. Chem., **67** (11) 2432 (1963).

[32] V. K. Tagirov, D. M. Chizhikov, E. K. Kazenas, and L. K. Shubochkin, Zh. Neorg. Khim., **20** (8) 2035 (1975).

[33] Y. Inoue, M. Hara, Y. Koyama, S. Ikeda, Y. Maeno, and T. Fujita, in "Advances in Superconductivity IX" (Springer-Verlag, Tokyo, 1997) p.165.

[34] J. S. Gardner, G. Balakrishnan, D. M^{c}K.Paul, and C. Haworth, Physica C **265**, 251 (1996).

[35] M. Braden, A. H. Moudden, S. Nishizaki, Y. Maeno, and T. Fujita, Physica C **273**, 248 (1997).

[36] Y. Morii, private communications.

[37] M. K. Crawford, M. A. Subramanian, R. L. Harlow, J. A. Fernandez-Baca, Z. R. Wang, and D. C. Johnston, Phys. Rev. B **49**, 9198 (1994).

[38] M. Itoh, T. Shimura, Y. Inaguma, and Y. Morii, J. Solid State Chem. **118**, 206 (1995).

[39] A. Kanbayashi, J. Phys. Soc. Jpn. **44**, 108 (1978).

[40] R. J. Bouchard, and J. F. Weiher, J. Solid State Chem. **4**, 80 (1972).

[41] M. Braden, G. André, S. Nakatsuji, and Y. Maeno, submitted to Phys. Rev. B.

[42] J. M. Longo, P. M. Raccah, and J. B. Goodenough, J. Appl. Phys. **39**, 1327 (1968).

[43] G. Aeppli, E. Bucher, C. Broholm, J. K. Kjems, J. Baumann, and J. Hufnagl, Phys. Rev. Lett. **60**, 615 (1988).

[44] K. Machida, private communications.

[45] G. R. Stewart, Z. Fisk, J. O. Williams, and J. L. Smith, Phys. Rev. Lett. **52**, 679 (1984).

[46] P. B. Allen, H. Berger, O. Chauvet, and L. Forro, T. Jarlborg, A. Junod, B. Revaz, and G. Santi, Phys. Rev. B **53**, 4393 (1996).

[47] A. P. Mackenzie, S. Ikeda, Y. Maeno, T. Fujita, S. R. Julian, and G. G. Lonzarich, to appear in J. Phys. Soc. Jpn. **67**, Letters No.2 (1998).

[48] Hk. Müller-Buschbaum, and J. Wilkens, Z. Anorg. Allg. Chem. **591**, 161 (1990).

[49] B. Batlogg, D. J. Bishop, E. Bucher, B. Golding Jr., A. P. Ramirez, Z. Fisk, J. L. Smith and H. R. Ott, J. Magn. & Magn. Matter. **63&64**, 441 (1987).

[50] A. P. Ramirez, B. Batlogg, E. Bucher and A. S. Cooper, Phys. Rev. Lett. **57**, 1072 (1986).

[51] T. Moriya, *Spin Fluctuations in Itinerant-Electron Magnetism* (Springer-verlag, 1985).

[52] T. Kiyama, K. Yoshimura, and K. Kosuge, Advances in Superconductivity IX edited by S. Nakajima and M. Murakami (Springer-Verlag, Tokyo, 1997) p. 171.

[53] M. Hatatani and T. Moriya, J. Phys. Soc. Jpn. **64**, 3434 (1995).

[54] Y. Takahashi, J. Phys. Soc. Jpn. **55**, 3553 (1986).

[55] Y. Takahashi, and T. Moriya, J. Phys. Soc. Jpn. **54**, 1592 (1985).

[56] Y. Takahashi, J. Phys. Condens. Matter **9**, 10359 (1997).

Table 1. Effective Bohr magneton number p_{eff}, Weiss temperature Θ_W and temperature independent term χ_0 for FZ crystals of $Sr_3Ru_2O_7$.

	H//ab	*H//c*
p_{eff}	2.52	2.99
Θ_W(K)	–39.4	–44.7
χ_0(emu/Ru mol)	3.64×10^{-4}	-5.21×10^{-5}

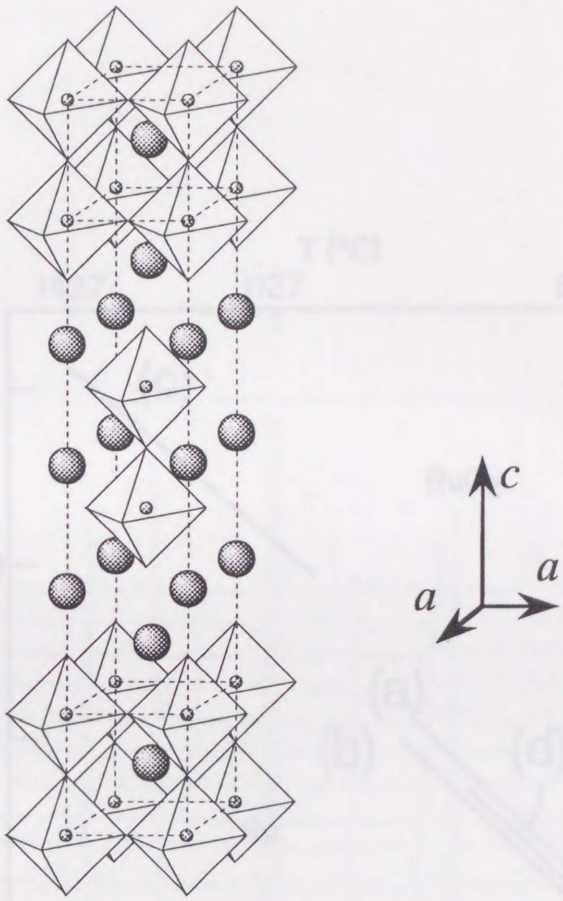

$Sr_3Ru_2O_7$

Fig. 1 . The crystal structure of $Sr_3Ru_2O_7$. The large circles represent Sr and small circles Ru. The cubes indicate RuO_6 octahedra.

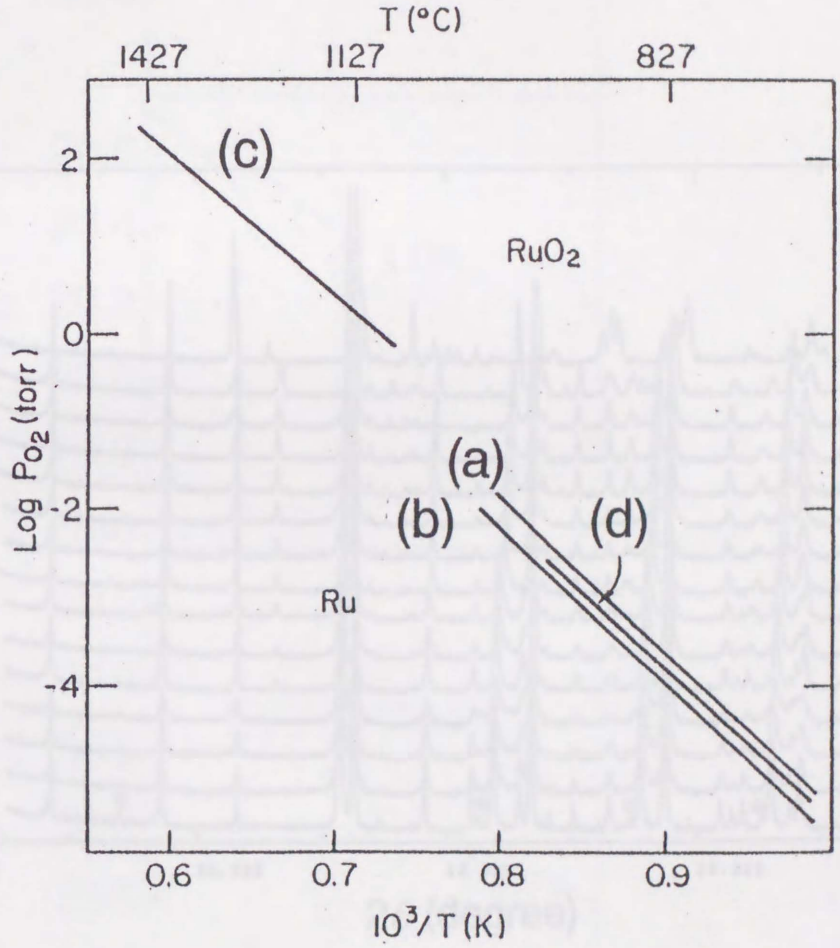

Fig. 2. Equilibrium pressure for the reaction $RuO_2 \rightarrow Ru+O_2$ investigated by several groups. (a) Ref. 29, (b) Ref. 30, (c) Ref. 31, (d) Ref. 32.

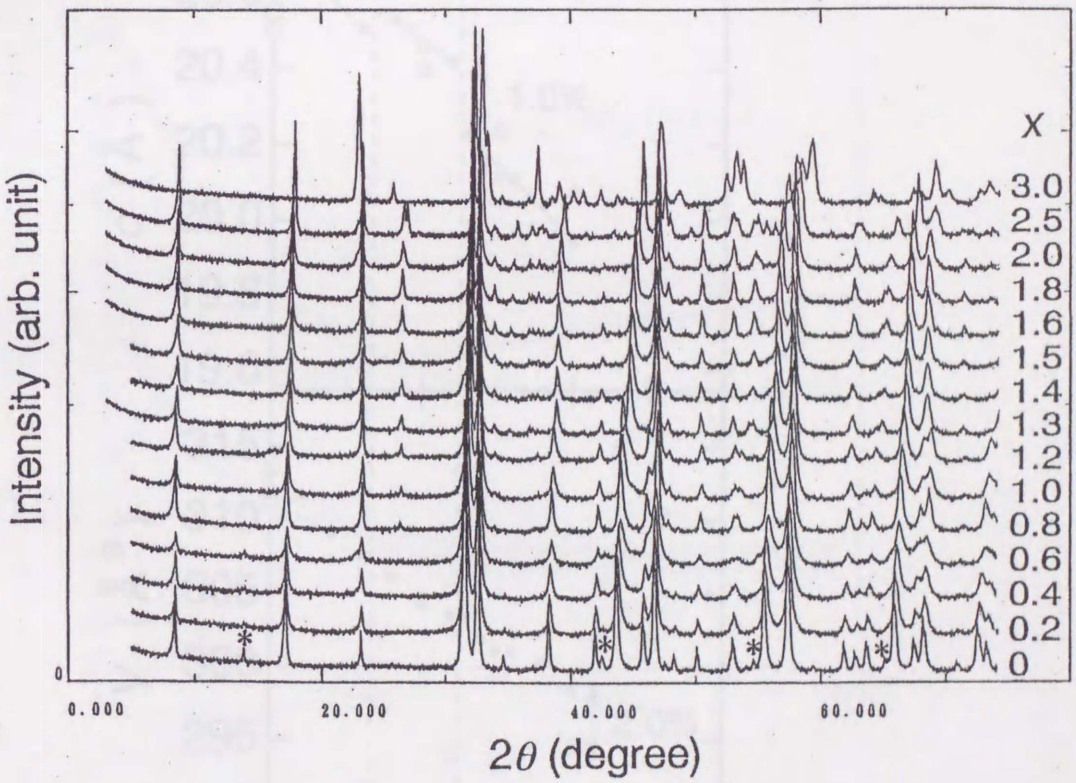

Fig. 3. X-ray powder diffraction patterns of $Sr_{3-x}Ca_xRu_2O_y$ with varying Ca concentration x. All peaks of $0 \leq x \leq 2.0$ are consistent with the symmetry of *I4/mmm*. The asterisks indicate Sr_2RuO_4 impurity.

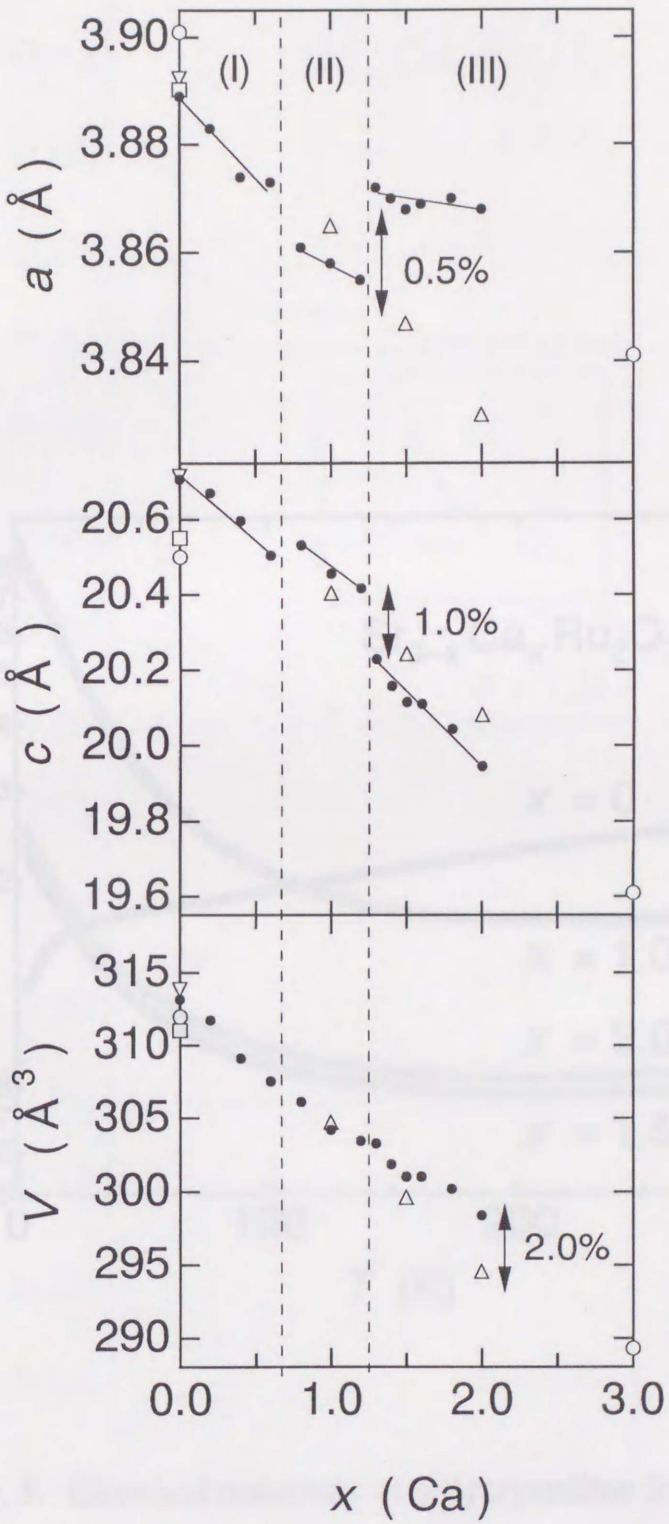

Fig. 4. The Ca concentration dependence of the *a* parameter, *c* parameter and unit cell volume. ● :as-prepared sample, △ :oxidized sample (present work), □ :flux-method single crystals (Müller-Buschbaum *et al.,* Ref.[48]), ▽ :polycrystals ,(Cava *et al.,* Ref.[17]), ○ :flux-method single crystals (Cao *et al.,* Ref.[22-24]).

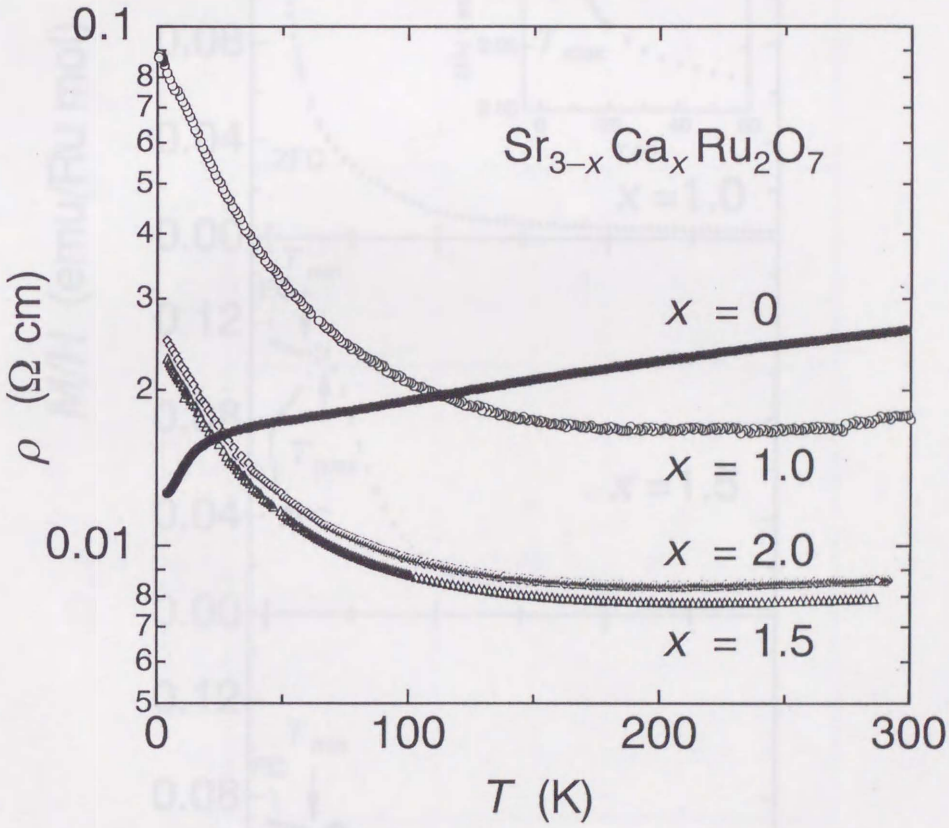

Fig. 5. Electrical resistivity of polycrystalline $Sr_{3-x}Ca_xRu_2O_7$.

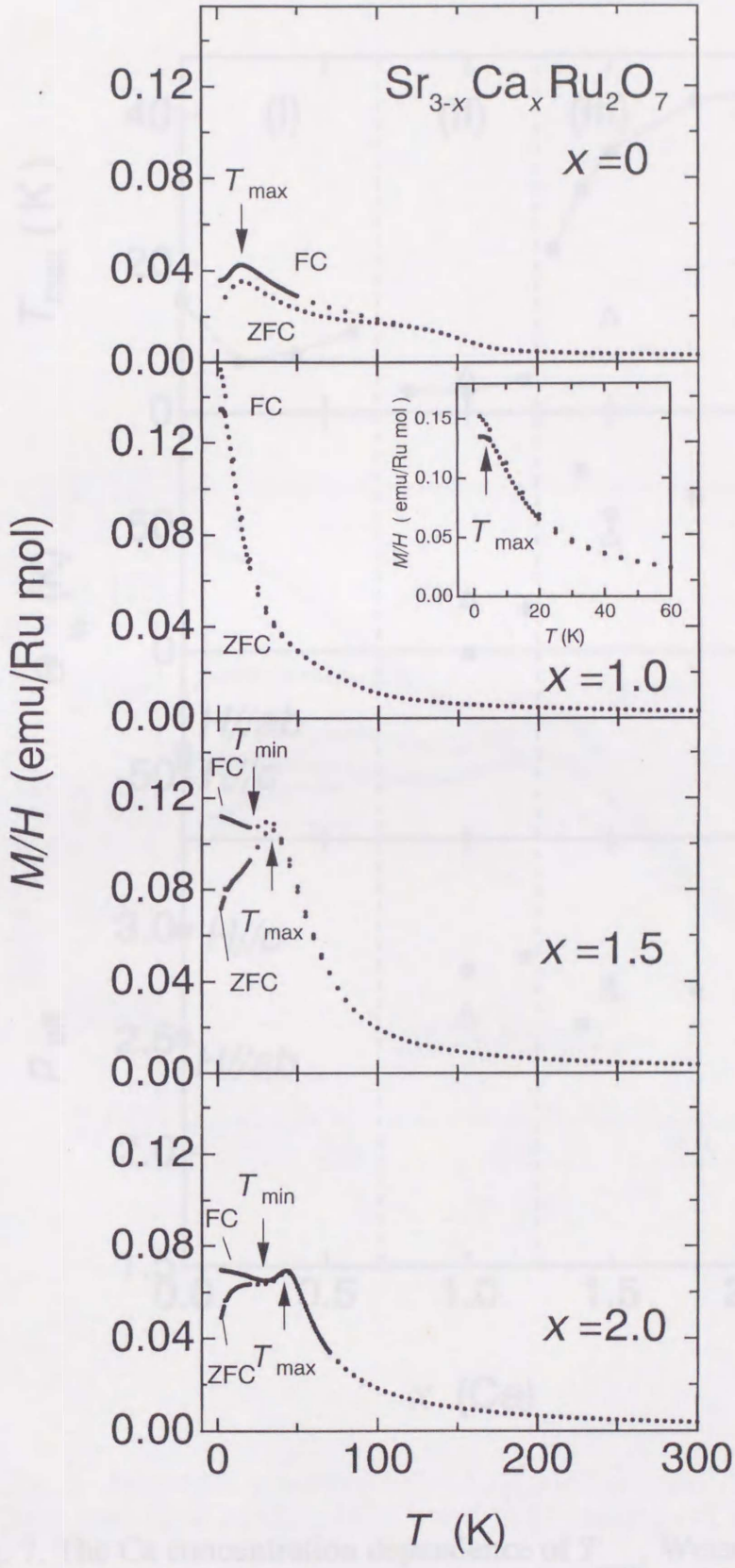

Fig. 6. Magnetic susceptibility under the field of 1T. Both zero field cooling (ZFC) and field cooling (FC) data are shown. Characteristic temperature T_{max} is defined as the temperature of the susceptibility maximum. See text for other notations.

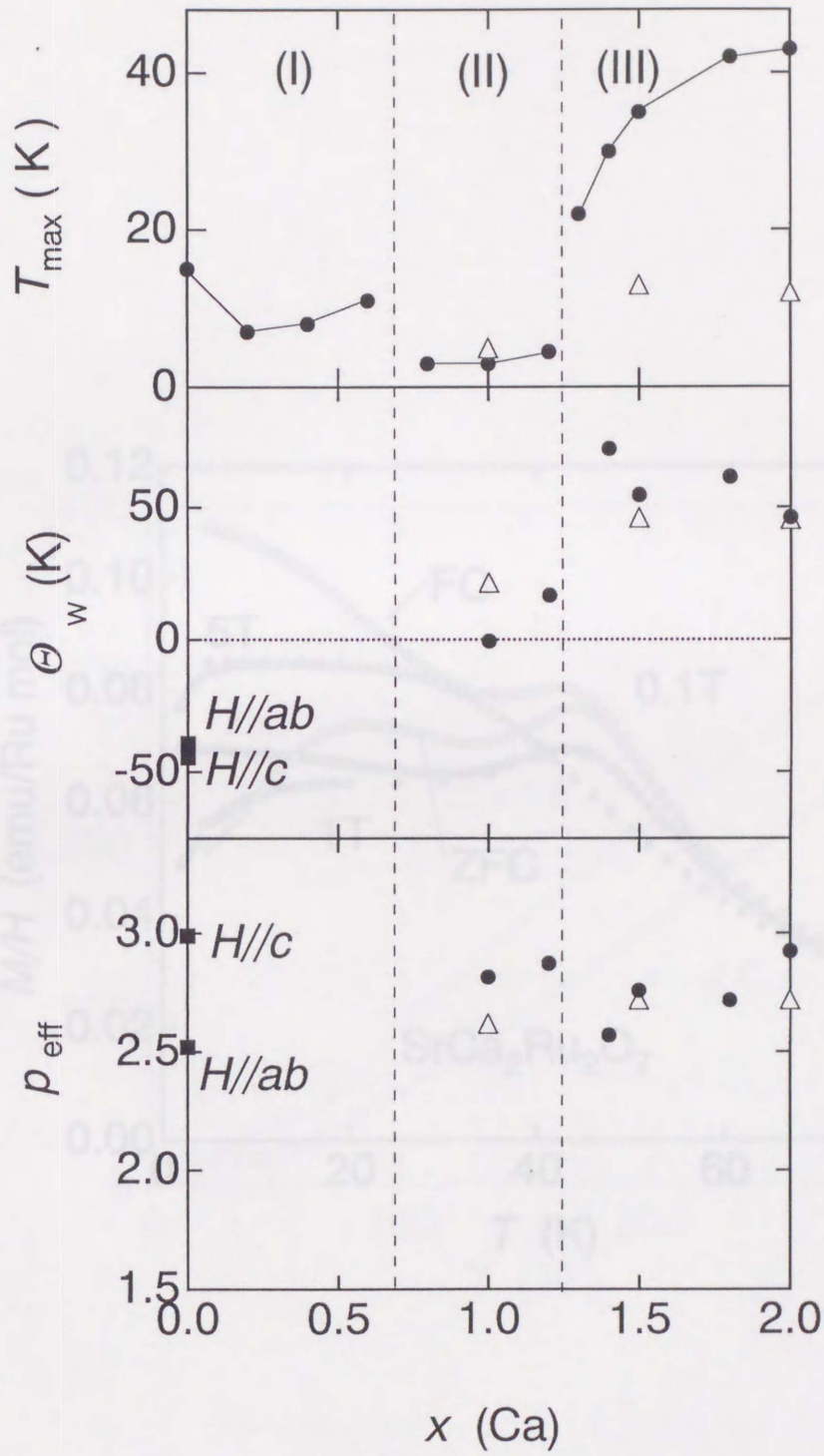

Fig. 7. The Ca concentration dependence of T_{max}, Weiss temperature Θ_W, and the effective Bohr magneton number p_{eff}. ● :as-prepared samples, △ :oxidized samples, and ■ :FZ single crystals.

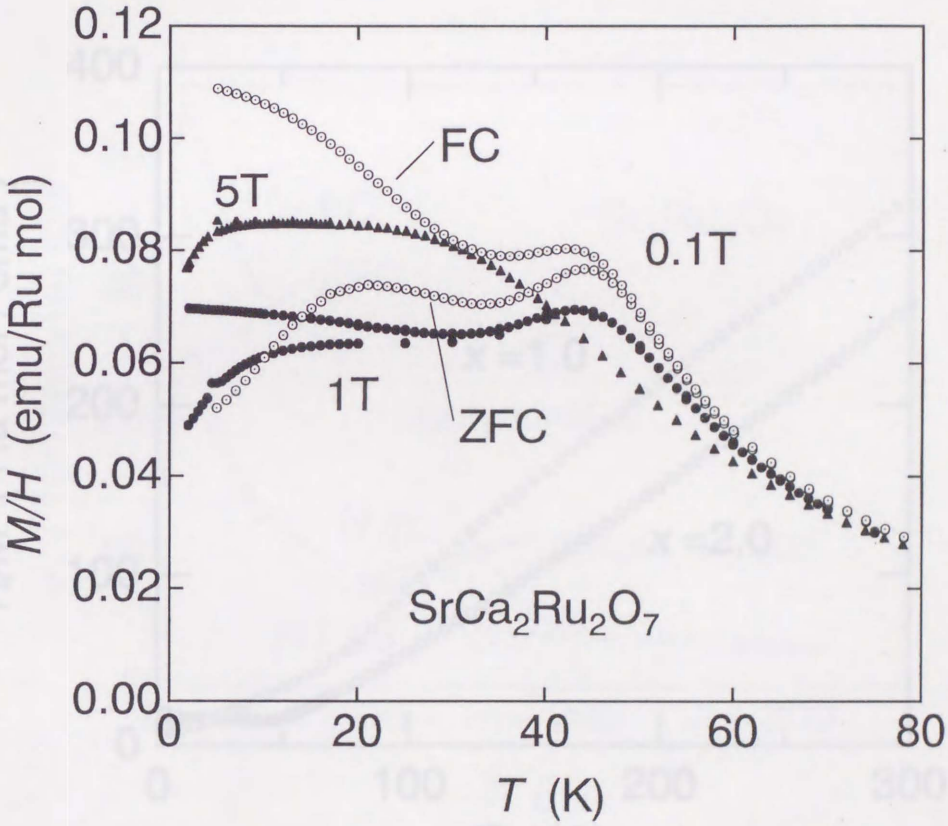

Fig. 8. Magnetic susceptibility of x(Ca)=2.0 under different fields. Both zero field cooling (ZFC) and field cooling (FC) data are shown.

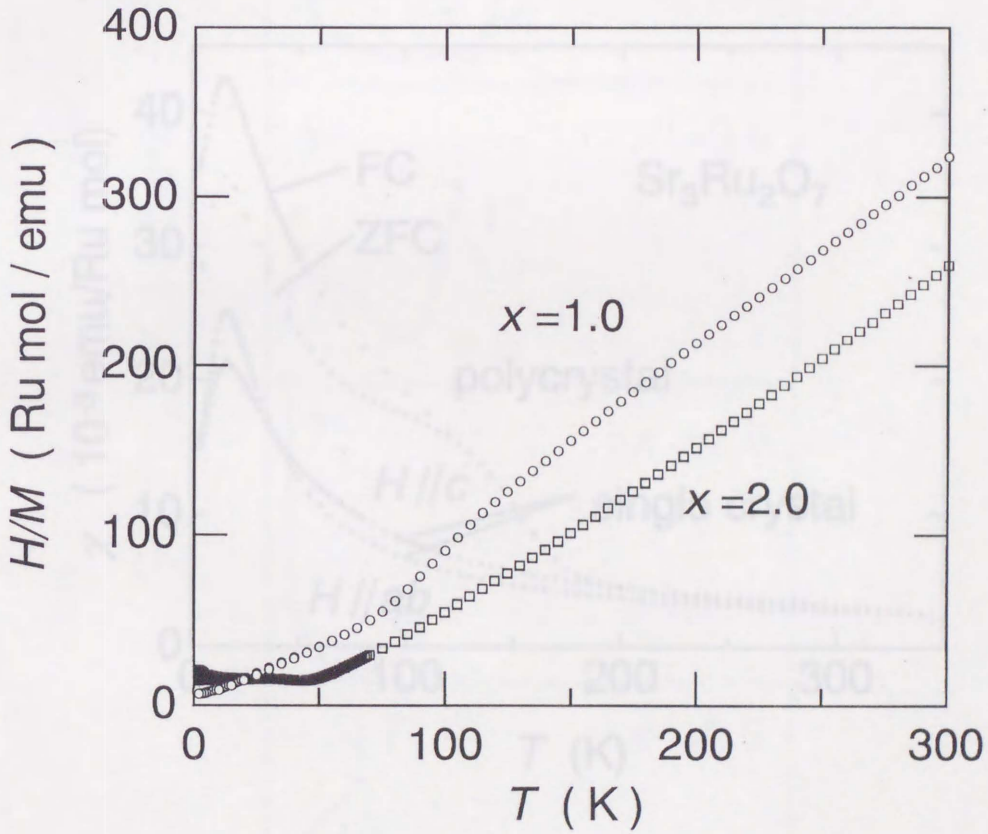

Fig. 9. The reciprocal magnetic susceptibility for x=1.0 and 2.0.

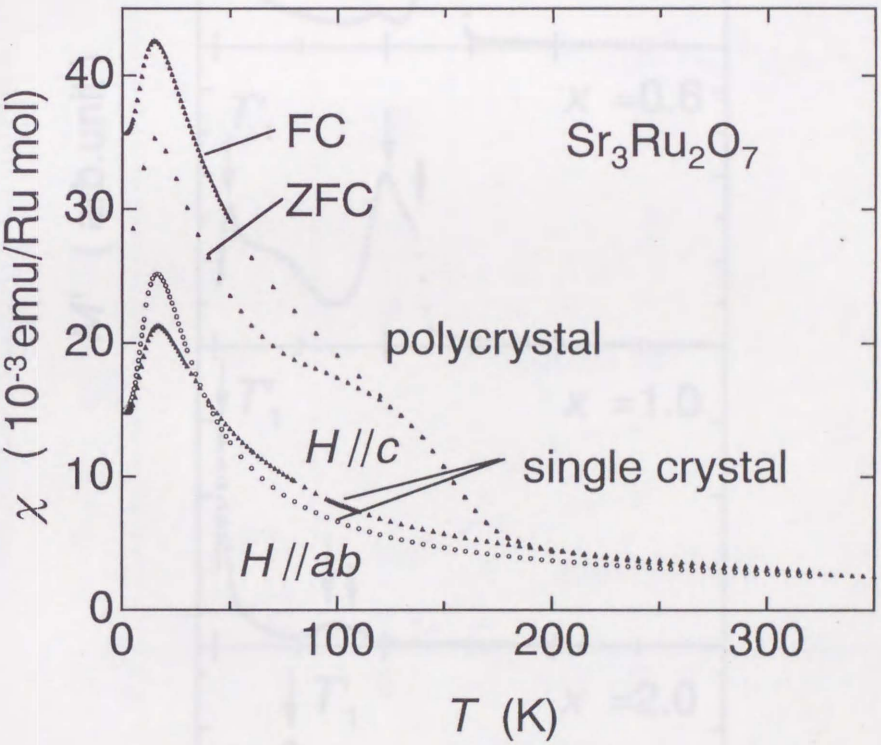

Fig. 10. Magnetic susceptibility of $Sr_3Ru_2O_7$ for both single crystals and polycrystals. The difference of susceptibility below 160 K is due to the ferromagnetic impurity $SrRuO_3$.

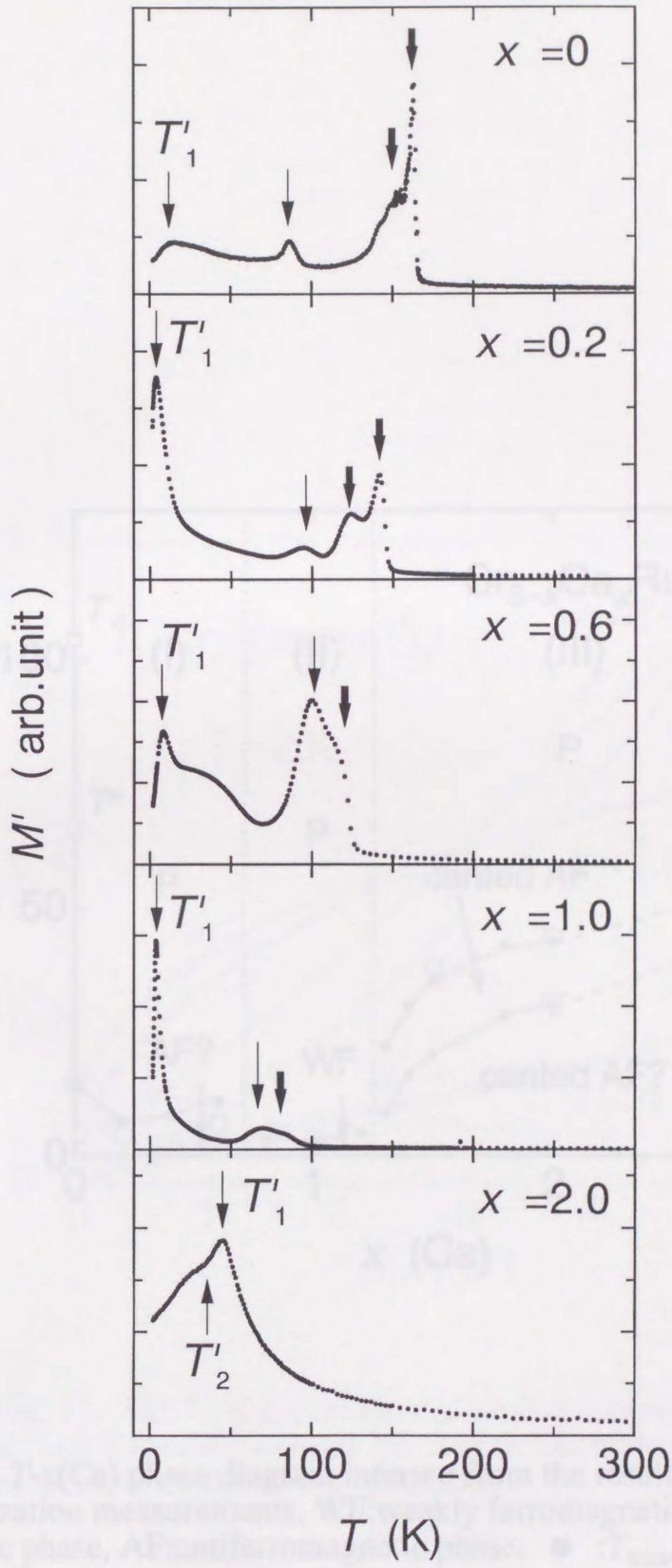

Fig. 11. The temperature dependence of AC magnetization M' for different x from 2 to 300 K. Thick arrows indicate the peaks due to (Sr,Ca)RuO_3 and thin arrows unidentified impurities.

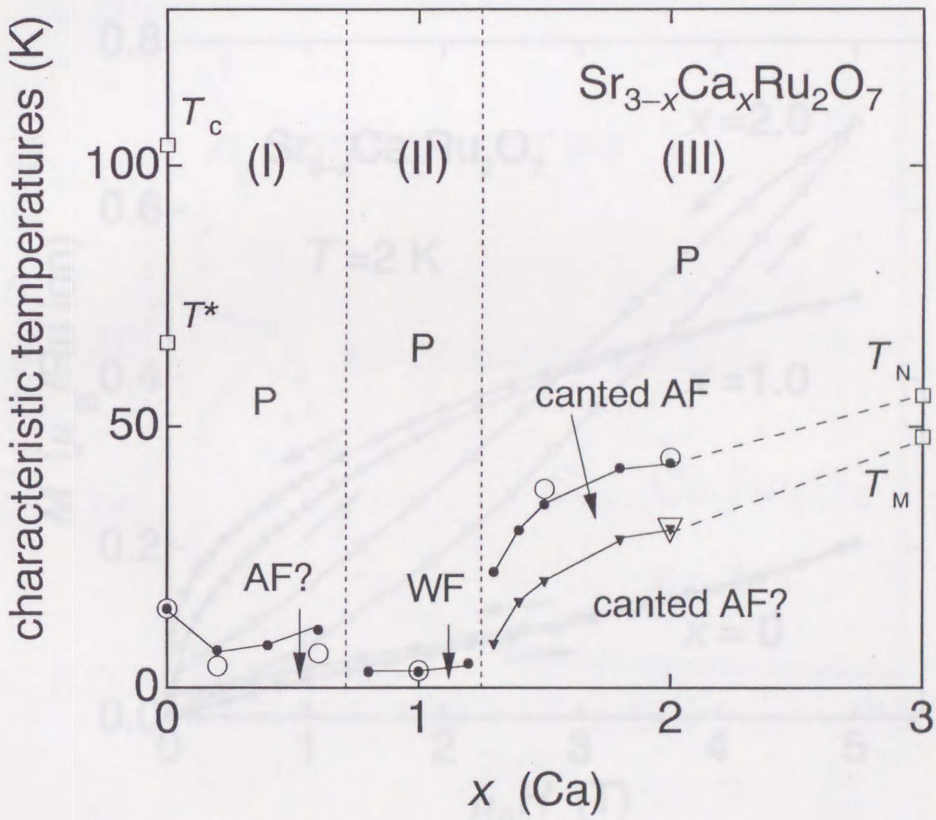

Fig. 12. T-x(Ca) phase diagram inferred from the results of DC and AC magnetization measurements. WF:weakly ferromagnetic phase, P:paramagnetic phase, AF:antiferromagnetic phase. ● :T_{max}, ▼ :T_{min}, ○ :T_1', ▽ :T_2', □ :characteristic temperatures defined for flux-method single crystals (Ref. [22,23]).

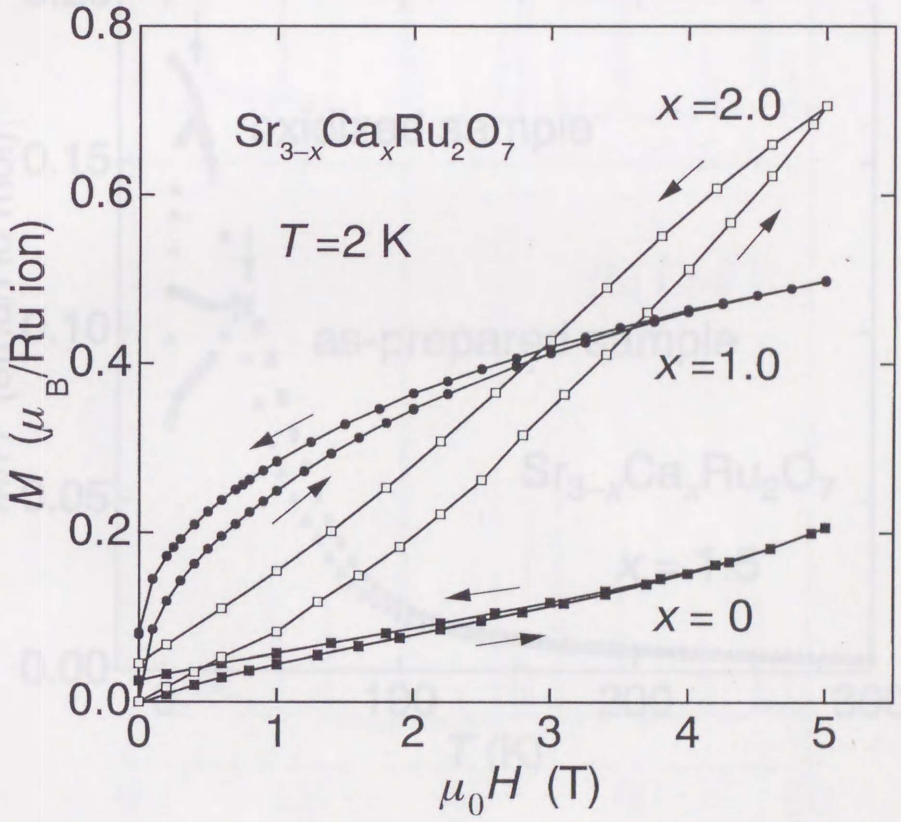

Fig. 13. The field dependence of magnetization at 2 K up to 5 T for x=0, 1.0 and 2.0. For x=1.0, quite different behavior from others are recognized.

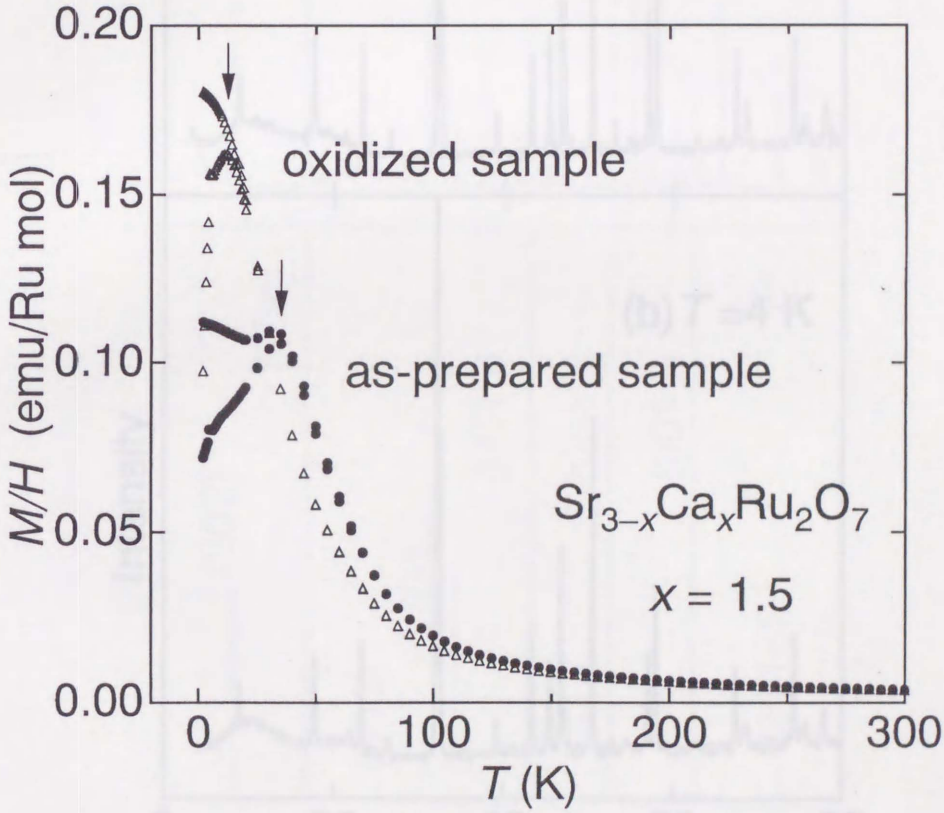

Fig. 14. Oxidation effects on $\chi(T)=M/H$ for x=1.5. The cusp observed in $\chi(T)$ of as-prepared sample in the FC curve is diminished by O_2 annealing.

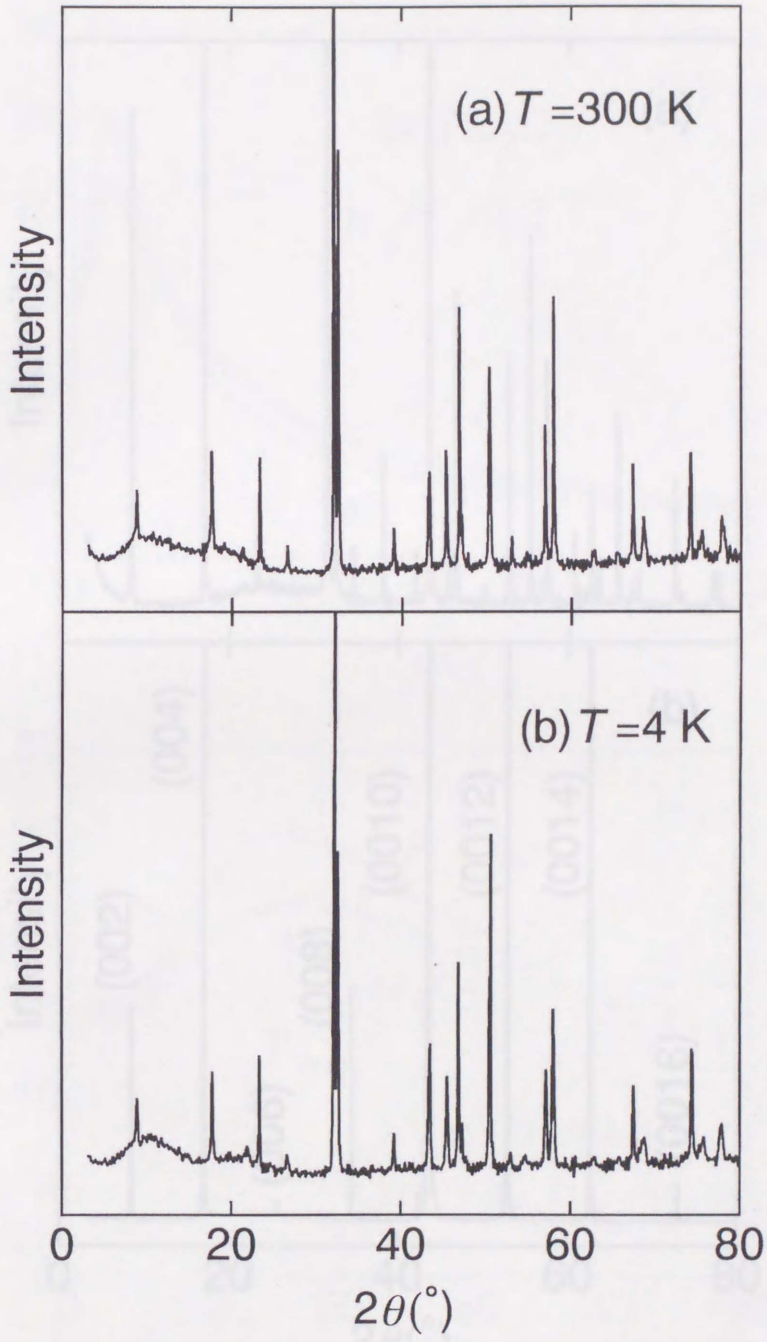

Fig. 15. Powder x-ray diffraction patterns of $SrCa_2Ru_2O_7$ at 300 K (a) and 4 K (b).

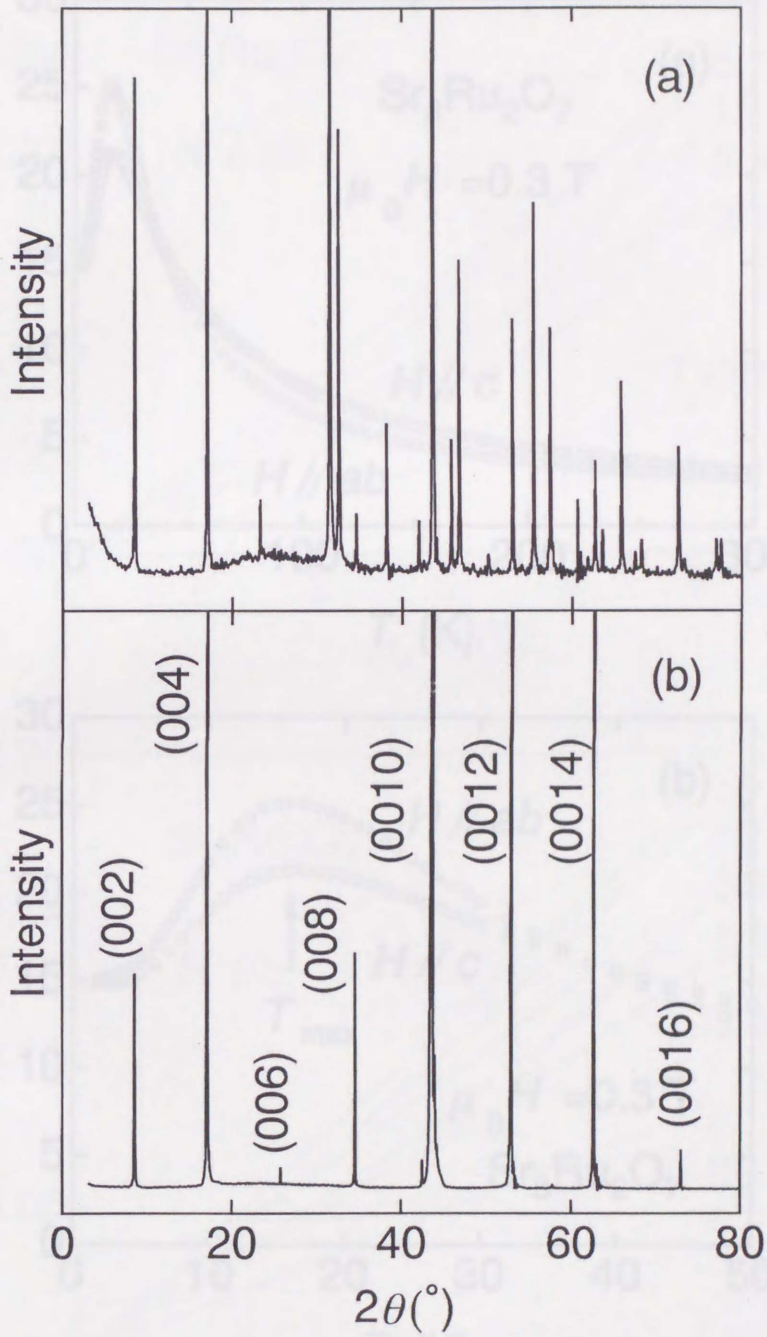

Fig. 16. X-ray diffraction spectrum (a) of powder and (00ℓ) reflection spectrum (b) of FZ crystals of $Sr_3Ru_2O_7$.

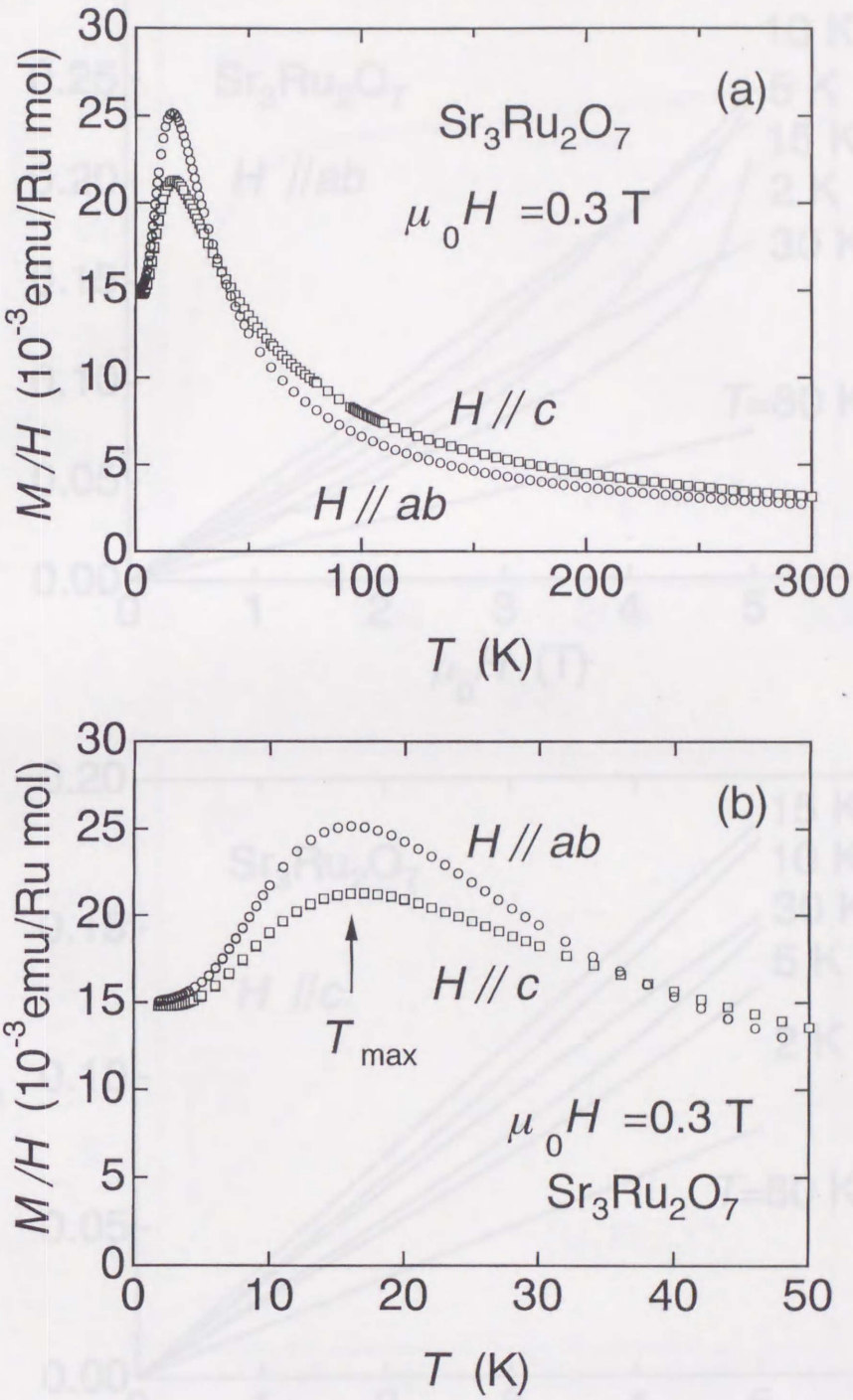

Fig. 17. Magnetic susceptibility of FZ crystals of $Sr_3Ru_2O_7$ under 0.3 T field in the range of (a)2-300 K and (b)2-50 K.

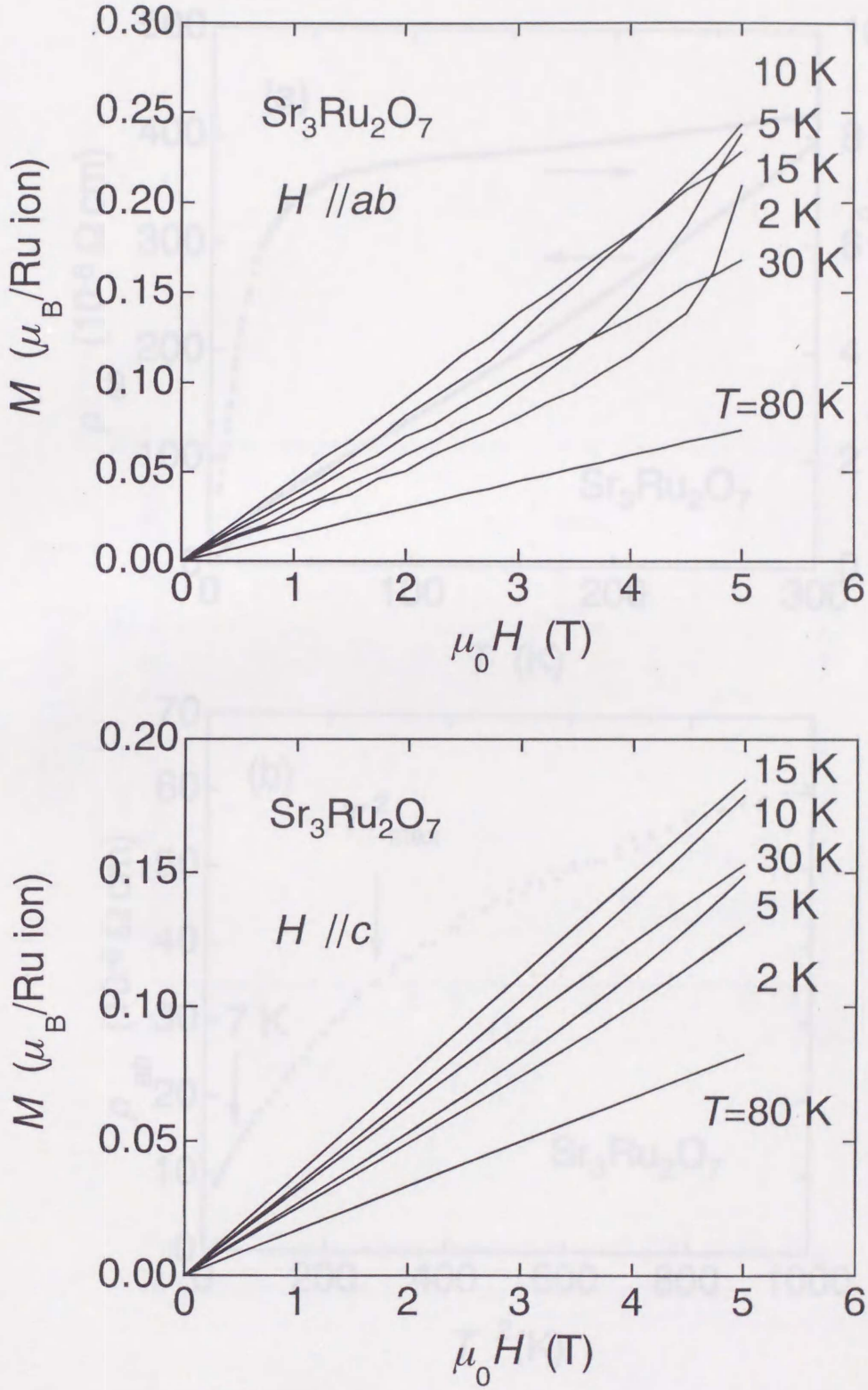

Fig. 18. Field dependence of magnetization M (H) of FZ single crystalline $Sr_3Ru_2O_7$.

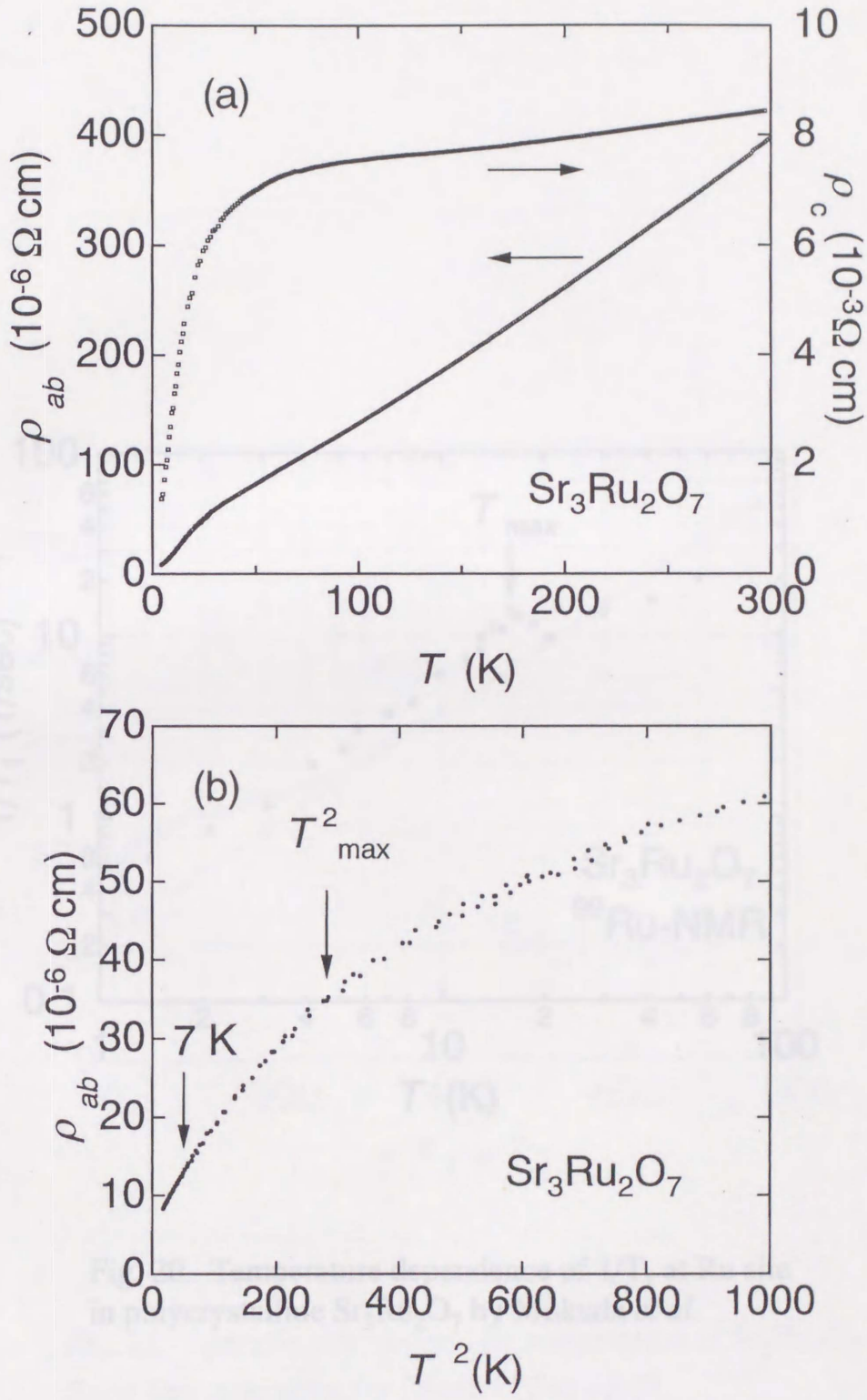

Fig. 19. (a) Electrical resistivity of FZ crystals of $Sr_3Ru_2O_7$ in the range of 4-300 K. Both ρ_{ab} and ρ_c are shown. (b) T^2-dependence of ρ_{ab} below 7 K.

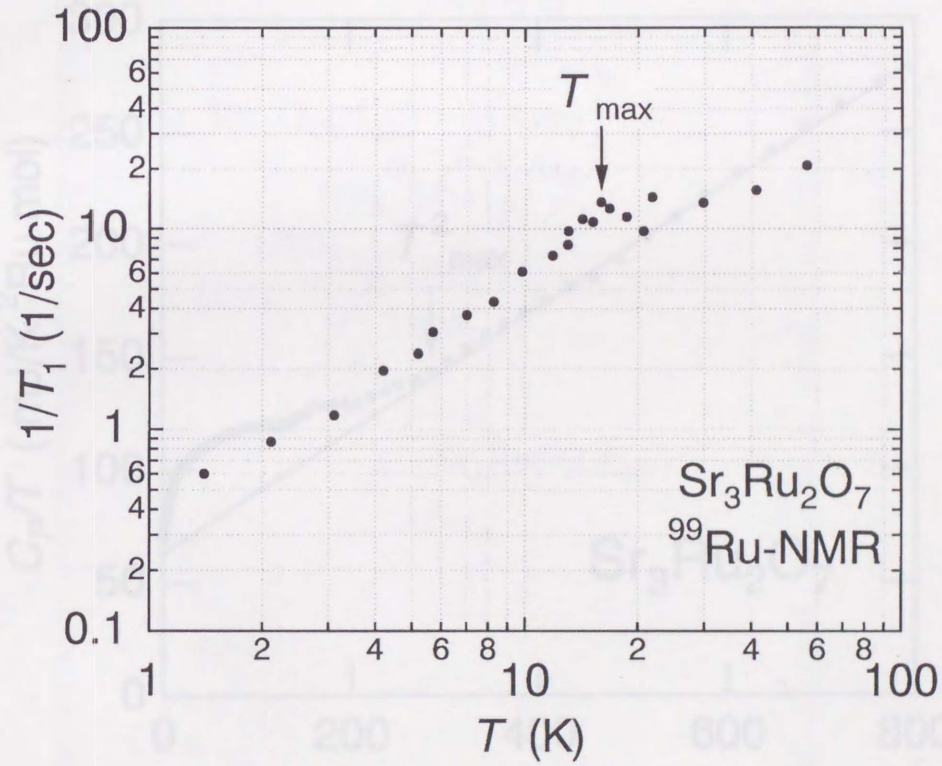

Fig. 20. Temperature dependence of $1/T_1$ at Ru site in polycrystalline $Sr_3Ru_2O_7$ by Mukuda *et al.*

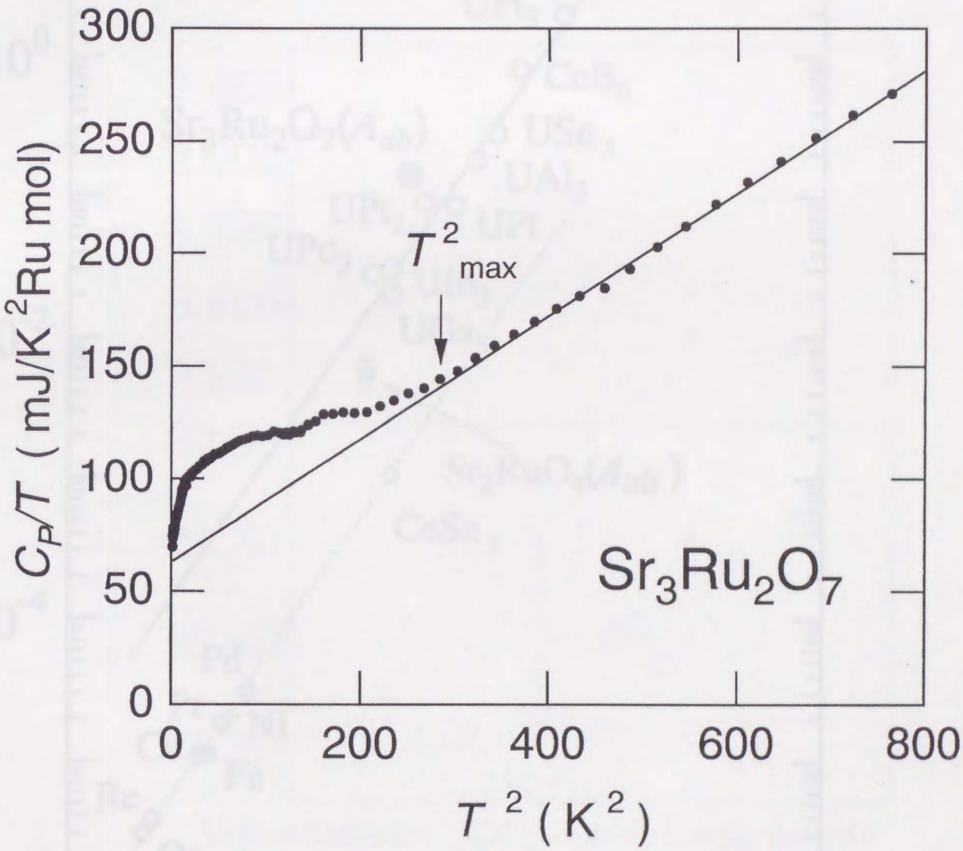

Fig. 21. Specific heat divided by temperature of $Sr_3Ru_2O_7$. Solid line represents the fitting $C/T=\gamma+\beta T^2$.

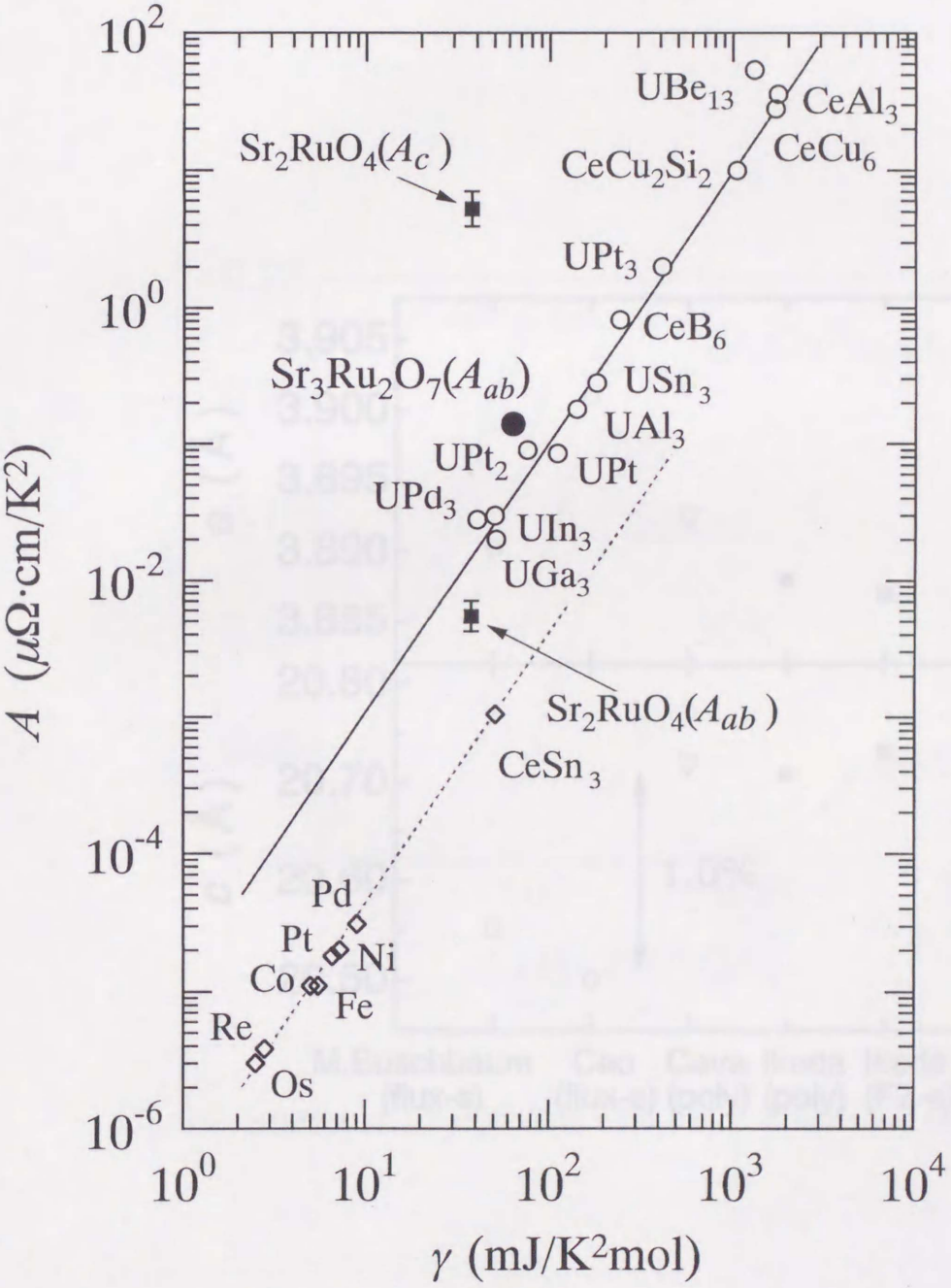

Fig. 22. The coefficient A of the T^2 term of the resistivity, plotted against the Sommerfeld coefficient γ of the specific heat for heavy fermion compounds and some transition metals. The solid and broken lines represent the Kadowaki-Woods ratio $A/\gamma^2=a_0=1.0\text{x}10^{-5}\,\mu\Omega\,\text{cm}/(\text{mJ/K}^2\text{mol})^2$ and $a_0/25$, respectively. Heavy fermion compounds follow the former universality.

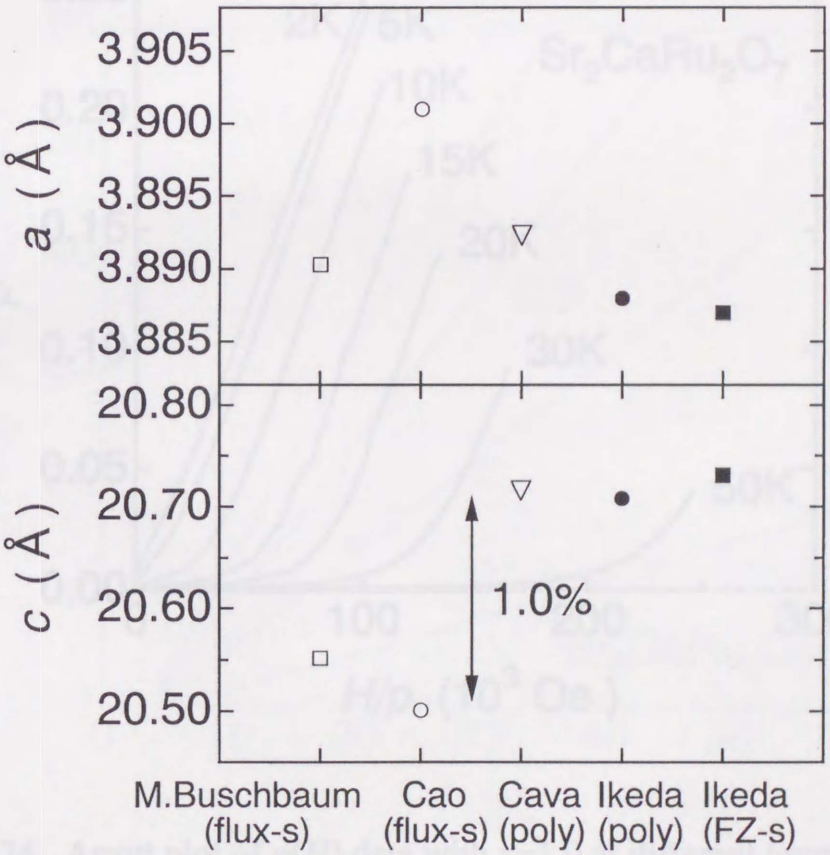

Fig. 23. Comparison of the lattice parameters of $Sr_3Ru_2O_7$ reported for different syntheses. □ :flux-method single crystals (Müller-Buschbaum *et al.* Ref.[48]), ○ :flux-method single crystals (Cao *et al.* Ref.[22,24]), ▽ :polycrystals (Cava *et al.* Ref.[17]), ● :polycrystals (present work), ■ :FZ crystals (present work).

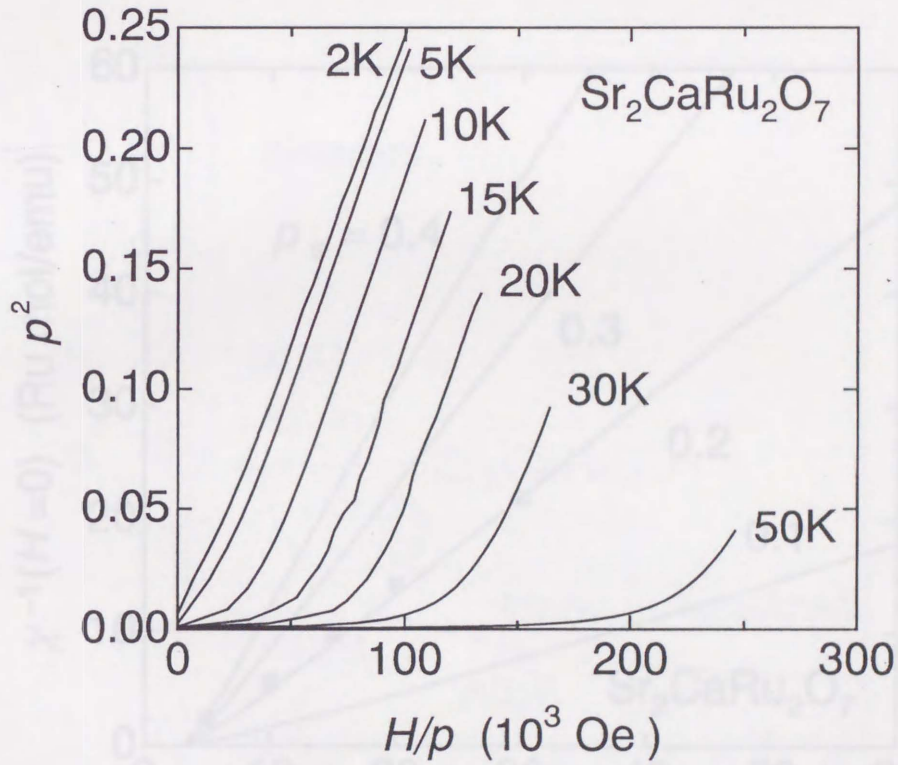

Fig. 24. Arrott plot of $p(H)$ data with x=1.0 at different temperatures.

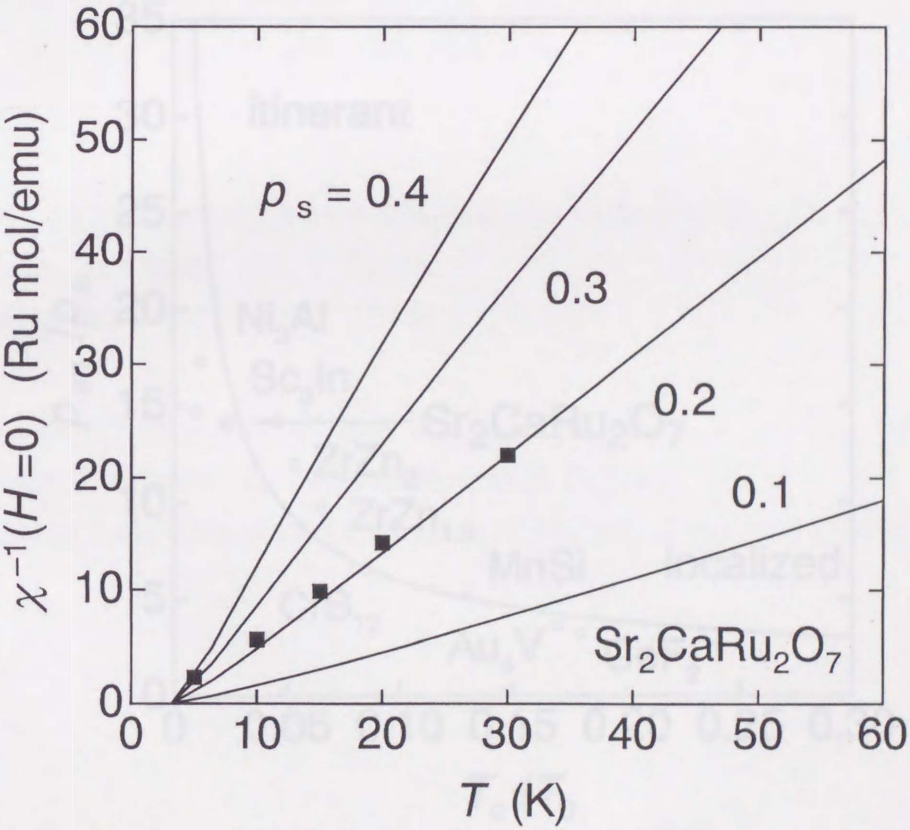

Fig. 25. Results of $\chi(T,H=0\ \mathrm{Oe})^{-1}$ calculated for x=1.0 by means of the SCR theory. The curves depend on parameters $\bar{F}_1$, T_c, T_0 and T_A in addition to p_s. Several different values for p_s are assumed and p_s=0.2 gives the best fit as shown.

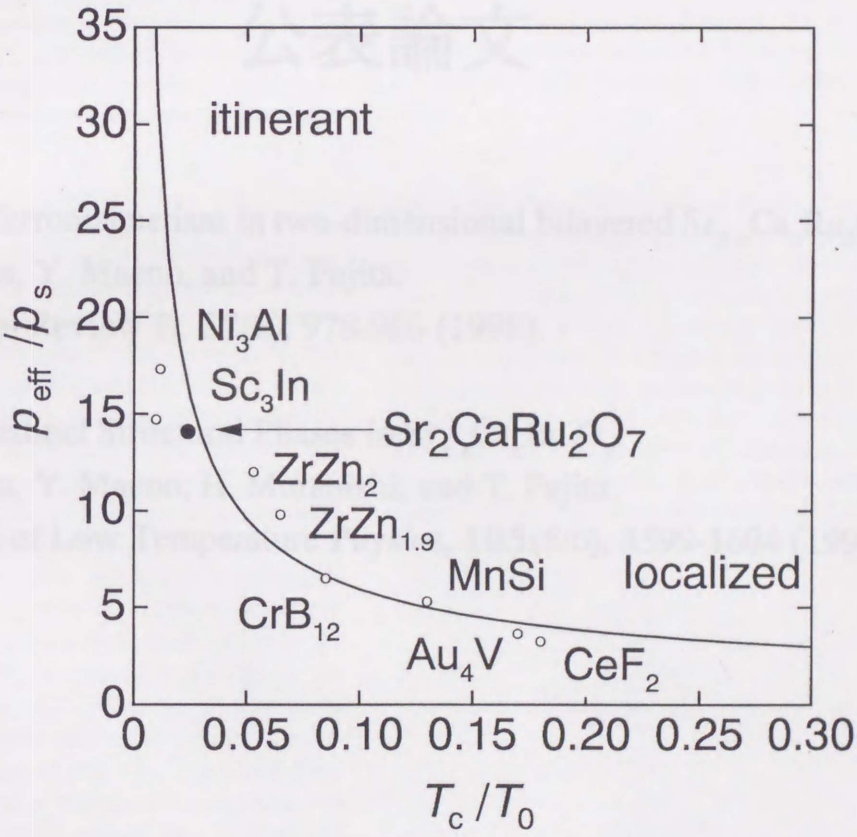

Fig. 26. Generalized Rhodes-Wohlfarth plots after Takahashi (Ref.[54]). The data of $Sr_2CaRu_2O_7$ is shown by a solid circle. Other intermetallic compounds are weak ferromagnets with three-dimensional crystal structure. Solid line is the theoretical expectation.

公表論文

(1) Weak ferromagnetism in two-dimensional bilayered $Sr_{3-x}Ca_xRu_2O_7$.
S. Ikeda, Y. Maeno, and T. Fujita.
Physical Review B, **57**(2), 978-986 (1998).

(2) Two Distinct Structural Phases in $Sr_{3-x}Ca_xRu_2O_y$.
S. Ikeda, Y. Maeno, H. Muranishi, and T. Fujita.
Journal of Low Temperature Physics, **105**(5/6), 1599-1604 (1996).

参考論文

(1) $Sr_2CaRu_2O_y$: a new phase of layered perovskite.
S. Ikeda, Y. Maeno, M. Nohara, and T. Fujita.
Physica C, **263**, 558-561 (1996).

(2) Ca_2RuO_4: New Mott Insulators of Layered Ruthenate.
Satoru NAKATSUJI, Shin-ichi IKEDA and Yoshiteru MAENO.
Journal of the Physical Society of Japan, **66**(7), 1868-1871(1997).

(3) Interplay between Kondo Effect and RKKY Interaction in $UCu_{3+x}Ga_{2-x}$.
S. Ikeda, S. Nishigori, T. Suzuki, T. Fujita,
Y. Maeda, T. Takabatake, and H. Fujii.
Physica B, **194-196**, 465-466 (1994).